

## **A Point-by-point Response to Review Comments**

Dear Dr. Feingold,

We are submitting the revised manuscript (#acp-2018-499) for your consideration of publication in *Atmospheric Chemistry and Physics*. We have carefully studied the reviewer's comments and revised the manuscript accordingly. Please find the point-by-point response (marked as blue) to the review comments. We have provided a copy of track-change manuscript as well as a clean copy of the revised manuscript.

Thank you for your consideration of this submission. We hope you find our response adequately address the review comments and the revision acceptable. We would greatly appreciate it if you could get back to us with your decision at your earliest convenience.

Sincerely,

Peng Wu

Department of Hydrology and Atmospheric Sciences

University of Arizona

Tucson, AZ 85721, USA

**Review of Wu et al., “Evaluation of autoconversion and accretion enhancement factors in GCM warm-rain parameterizations using ground-based measurements at the Azores,” first revision**

I must start by acknowledging the major effort undertaken by the authors to address my comments on the initial submission, especially with respect to obtaining collocated, vertically-resolved cloud and rain liquid water contents. I’m sure this was a significant undertaking, but it puts the premise of their analysis on solid footing and gives me much greater confidence in their conclusions. The addition of Appendix A to demonstrate the rain water content retrieval is also greatly appreciated. I still have a number of minor comments and there remain many language issues that introduce ambiguity in interpreting the authors’ statements. I therefore recommend **acceptance pending minor revisions** to address these comments, and I **strongly** recommend the authors use a professional copyediting service to handle the language issues.

Thanks for the insightful comments and suggestions for this and the initial submission, which helped to improve the manuscript a lot.

We have made point-to-point revisions and did a thorough proofreading for the revised manuscript.

**Other general comments:**

- It’s misleading that you call the effective length scale calculated from (wind speed \* time elapsed) a “model grid size.” It would be more accurate to use language such as “equivalent grid size” or “equivalent model grid size.”

- There is a pervasive units issue. Almost everywhere that grid size is given as an area, the units are given in km where they should be km<sup>2</sup>. Please correct throughout the manuscript or change all instances to “horizontal grid size of X km” such that they do not reference an area.

Thanks for the suggestions.

We have changed the terminology to ‘horizontal equivalent grid size’. For simplicity and convenience, it is referred to as ‘equivalent size’ in the text.

- Using a constant value of DSD width is analogous to using a constant LWC distribution width or  $E_{\text{auto}}/E_{\text{accr}}$  width – the spectral width of the DSD is something that varies (increases) with length scale (e.g. Geoffroy et al, 2010, ACP) and is also dependent on the choice of in situ instrumentation (e.g. Witte et al., 2018, GRL; also mentioned but not dealt with in Miles et al., 2000, JAS). While I don't think there's an obvious "better" solution at this point (the math would get considerably hairier if one also considers variable DSD shape), I think it’s important to note that by making this assumption, you're essentially just kicking the use of "parameters constant with length scale" down the line from LWC distributions to DSD width. This seems particularly prescient given that your argument for regime-dependence is reflected in the finding of Miles et al. (2000) that the distribution of DSD parameters is different for marine and continental clouds.

Thanks for the comment.

The assumed DSD width is used to retrieve LWC within a radar range gate and it is important to note that the LWC within a radar range gate is a bulk property and do not have a distribution.

The qc distribution within a specific time interval is used in the Gamma fitting and this distribution do not have a constant width and is little affected by the constant width of DSD. However, we agree with the reviewer that DSD width should vary with different sampling length/time and different instruments. We added the following discussion in Append A to feather this: ‘Geoffroy et al. (2010) suggested that  $\sigma_x$  increases with the length scale and Witte et al.

(2018) showed that  $\sigma_x$  also dependent on the choice of instrumentation. The variations of  $\sigma_x$  should be reflected in the retrieval by using different  $\sigma_x$  values with time. However, no aircraft measurements were available during CAP-MBL to provide  $\sigma_x$  over the Azores region. The inclusion of solving  $\sigma_x$  in the retrieval adds another degree of freedom to the equations and complicates the problem considerably. In this study,  $\sigma_x$  is set to a constant value of 0.38 from Miles et al. (2000), which is a statistical value from aircraft measurements of marine low-level clouds.'

**Specific content-related comments** are given in the remainder of the review in reference to page and line number(s) (format: PX, LY-Z = page X, lines Y-Z). Please see the annotated PDF following these comments for a non-comprehensive list of language issues.

P1, L33: This sentence gives the impression that there is a particular value that the qr-qc ratio should be. Be more explicit here about why this value matters – just throwing out the values without context (e.g. observed vs. typical GCM values) doesn't "prove" that the presently-used constant enhancement factors are wrong.

Thanks for the comment.

This sentence has been revised to 'The ratios of rain to cloud water mixing ratio at  $E_{accr}=1.07$  and  $E_{accr}=2.0$  are 0.063 and 0.142, respectively, from observations, further suggesting that the prescribed value'.

P3, L55: How do aerosol effects being tied to precipitation suppression fit with the rest of your argument? I fail to see the relevance, especially since your results show that precipitation frequency has almost no relationship with  $E_{auto,Ne}$ .

Thanks for the comment. This sentence has been deleted.

P4, L60-62: I don't see the point of this sentence. If you're getting at the idea that the "cloud" and "rain" sub-categories are an arbitrary division by drop size, say so.

Thanks for the comment.

This sentence is an elaboration of the parameterized rather than resolved process in GCMs and uses warm rain process as an example. We do not intend to explain the separation of rain and cloud sub-categories here.

P4, L72: Is there not one single study that parameterizes accretion as something other than a power law? You're on firmer ground saying "The vast majority" or something like that because it only takes one counterexample to make your statement false.

Thanks for the comment.

This sentence has been rephrased in the revised manuscript.

P5, L91-93: Cheng and Xu's autoconversion equation is independent of vertical velocity and rain mixing ratio (Text in right column of pg 2319 and their Eq. 6).

Thanks for the comment. This sentence has been revised.

P6, L 109: Why is recognition of spatial scales the important aspect? This seems trivial. Please expand.

Thanks for the comment.

Because the inhomogeneity parameter, similar as the enhancement factor in this study, characterizes cloud field in a grid. An inhomogeneous cloud in a GCM grid can be homogeneous in a WRF grid. Also, in the lon-lat grid setting GCMs the grid size can be dramatically different in tropical and polar regions. The inhomogeneity parameter in Xie and Zhang (2015) can be applied to the globe without manually tuning.

We expanded the following in the revised manuscript: "...found that it can recognize spatial scales without manual tuning and can be applied to the entire globe".

P6, L113-114: Do you mean Zhang et al. derived sub-grid distributions or the actual pixel-scale CLWP and  $N_c$ ? Please clarify.

Thanks for the comment.

Zhang et al. (2018) derived sub-grid distributions of CLWP and  $N_c$  and describe them using lognormal and gamma distributions. This is clarified in the revised manuscript.

P7, L131-132: Enhancement factors are applied at the grid scale by definition, so it seems repetitive to say "grid-mean process enhancement factors."

Thanks for the comment.

This has been rephrased to 'enhancement factors' in the revised manuscript.

P15, L268: You don't show  $q_r$  in Fig 1. Either reference rain LWC as shown in Fig. A1 or remove "and  $q_r$ " from the sentence.

Thanks for the comment.

This sentence has been rephrased to '...as seen from WACR reflectivity and  $q_r$  in Figure A1.' in the revised manuscript.

P17, L305: What does "relative constant" mean? Clarify what the adjective means or remove it.

Thanks for the comment. This has been removed.

P18, L317-319: There are a number of other explanations for this result: the dependence of autoconversion parameterizations on number concentration may be flawed, there could be problems with your number concentration retrieval, or perhaps the assumption of constant  $N_c$  with height doesn't work. Unless you have evidence that a) there is significant subgrid variability of  $N_c$  and b) it matters at the process level, I don't think you can make this statement.

Thanks for the comment. We decided to delete this statement in the revised manuscript.

P22, L402-404: The differences from prescribed values only have explanatory power if the simulations used to diagnose it were run at something comparable to 30 km horizontal resolution. Do you have a reference to support this?

Thanks for the comment.

The problem of 'too frequent and too light' is most prominent for the equivalent size of 30-km from the aspect of enhancement factors. We are not aware of any reference that draw similar conclusion.

P22, L410: The language "...the location we choose to collect ground-based observations..." implies that the authors were the primary decision makers regarding the location of the CAP-MBL deployment. If this is the case, this wording is fine. Otherwise, considering alternate

wording, e.g. "...the location of the ground-based observations and retrievals used in this study is..."

Thanks for the comment. This sentence has been re-written in the revised manuscript.

P25, L464: Use the  $180^2 \text{ km}^2$  value here for consistency. You use  $120^2 \text{ km}^2$  here while you show a maximum grid size of  $180^2 \text{ km}^2$  in the figures and use this same maximum grid size in reference to Eaccr below.

Thanks for the comment.

This sentence has been changed in the revised to 'The calculated  $E_{auto}$  values from observations and retrievals increase from 1.96 at an equivalent size of 30 km to 3.18 at an equivalent size of 150 km. These values are 38% and 0.625% lower than the prescribed value of 3.2. The prescribed value in MG08 represents well in large grid sizes in GCMs (e.g.,  $180^2 \text{ km}^2$  grid).' in the revised manuscript.

P28, L519-520: This sentence is confusing. I think you're trying to say "if the vertical gradient of  $N_w$  is negative below cloud base" - can you confirm?

Thanks for the comment.

Yes, if the  $N_w$  vertical gradient below cloud base is negative, we use constant  $N_w$  in cloud.

This sentence has been rephrased in the revised manuscript.

P29, L526-527: Italicize all instances in the text of  $Z$  ( $Z_c$ ,  $Z_d$ , etc.). Also, does the subscript "d" indicate drizzle? You use the subscript "r" in Eq. A1 and elsewhere in the main manuscript.

Thanks for the comment. These have been changed in the revised manuscript.

P29, L530: Rearrange Eq. A2 for the value you're actually solving for ( $CLWC(1)_{reflectivity}$ ).

Thanks for the comment. The equation has been rearranged.

P29, L536: Eq. A2 only gives reflectivity at cloud base. How do you integrate up for the profile?

Thanks for the comment. The reflectivity is calculated from the updated adiabatic LWC (after multiplying by  $s$ ). for clarification, the sentence is rephrased as 'Reflectivity profile from cloud is then calculated from Eq. (A2.1) using the updated  $CLWC_{adiabatic}$ '.

P30, L543-544: What if there is no drizzle at cloud top? How good is the assumption that you can just decrease  $N_w$  until your criteria is satisfied?

Thanks for the comment. The big assumption in the rain estimation method is that, whenever rain occurs below cloud base, it exists in the whole cloud layer. This assumption may not hold in situations that the top layer is affected by entrainment and no rain drops exist. However, without in situ measurement, we are unable to identify if rain drops exist near cloud in a case by case base.

The minimum value of  $N_w$  at the top layer in our estimation is on the order of  $10^{-4}$ , which is considered a good approximation to the situation that  $N_w$  is zero and this approximation has little effect on the reflectivity calculation.

Table 2 (P 42, L819): While visually repetitive, the table is more readable if the upper left corner cell is clear. The entries in the leftmost column should then read (from top to bottom):  $LTS > 18$

K,  $13.5 < LTS < 18$  K,  $LTS < 13.5$  K. You may also consider placing a vertical line between the first and second columns to differentiate between the category column and results/data.  
Thanks for the comment. Table 2 has been changed in the revised manuscript.

Figure 1, panel c (P44, L825): Why does the histogram look so much different than the fitted gamma distribution? Assuming 5-10 m/s wind speeds there would be something like 60-120 samples for an equivalent 60 km scale, so is this just a consequence of coarse binning?  
Thanks for catching this. It was a mistake in our plotting code. The figure has been updated in the revised manuscript.

Figure 1 caption (P44, L 832): Replace “mean-qc” with an overbar over qc.  
Thanks, this is changed.

Figure 2, panels e-f (P45, L 839): The label “cov(qc, qr)” is misleading because you don’t actually show the covariance anywhere.

Figure 2, panels e-f (P45, L839): Consider adding minor ticks to the y axes or plot the ratios on a separate right axis. It’s very difficult to get a sense for the maximum magnitude of qr/qc because it’s all below the 0.2 tick.

Figure 2 (P45, L839): Add labels to the y axes to show that both the PDF and (precip frequency/qr-qc ratio) are shown on the same scale, i.e. label y axes “PDF, precipitation frequency” and “PDF, qr-qc ratio” or similar. This information shouldn’t be buried at the bottom of the caption.

Thanks for the comment. We have changed cov(qc, qr) to qc, qr, changed y-axis label and added minor ticks in the revised manuscript.

Figure 5 (P48, L856): How do these adjustments compare with retrieval uncertainty? I ask because you show in Fig. 4 that uncertainty in E decrease with equivalent grid size. For example, if the retrieval uncertainty at 30 km is 20%, then does a qc adjustment tell you something physical or is it just another way of describing uncertainty?

Thanks for the comment.

We do not think the percentages in Figure 5c is a direct result of retrieval uncertainty. Rather, the percentages in Figures 5a and 5b may result from uncertainties of qc retrieval. For example, for the 60-km equivalent size, the broad range from -40% to 40% is the actual adjustment and is greater than the retrieval error.

The averaged adjustment for 180-km equivalent size is zero but the uncertainty in Eaccr is comparable to the 60-km equivalent size.

This figure should be considered as another way of demonstrating the information in Figure 4. If the retrieval uncertainty is to be considered, a similar shaded area as in Figure 4 should be around the solid line in Figure 5c.

1**Evaluation of autoconversion and accretion enhancement factors in GCM warm-rain**  
2**parameterizations using ground-based measurements at the Azores**

3Peng Wu<sup>1</sup>, \*Baiké Xi<sup>1</sup>, Xiquan Dong<sup>1</sup>, and Zhibo Zhang<sup>2</sup>

4<sup>1</sup> Department of Hydrology and Atmospheric Sciences, The University of Arizona, Tucson,  
5Arizona, USA

6<sup>2</sup> Physics Department, The University of Maryland, Baltimore County, Maryland, USA

7

8

9 Submitted to Atmospheric Chemistry and Physics (~~September 17~~November 21,  
102018)

11

12

13**Keywords:** MBL clouds, enhancement factors, autoconversion and accretion parameterizations

14

15

16

17

18

19\* Corresponding author address: Dr. Baiké Xi, Department of Hydrology and Atmospheric  
20Sciences, University of Arizona, 1133 E. James E. Rogers Way, Tucson, AZ 85721-0011.

21baikexi@email.arizona.edu; Phone: 520-626-8945

## 22 Abstract

23 A great challenge in climate modelling is how to parametrize sub-grid cloud processes, such  
24 as autoconversion and accretion in warm rain formation. In this study, we use ground-based  
25 observations and retrievals over the Azores to investigate the so-called enhancement factors,  
26  $E_{auto}$  and  $E_{accr}$ , which are often used in climate models to account for the influences of sub-grid  
27 variances of cloud and precipitation water on the autoconversion and accretion processes.  $E_{auto}$   
28 and  $E_{accr}$  are computed for different equivalent model grid resolution sizes. The calculated  $E_{auto}$   
29 values increases from 1.96 (30 km) to 3.245 (1280 km), and the calculated  $E_{accr}$  values increase  
30 from 1.53 (30 km) to 1.76 (180 km). Comparing the prescribed enhancement factors in  
31 Morrison and Gettleman (2008, MG08) to the observed ones, we found that a higher  $E_{auto}$  (3.2)  
32 at small grids and lower  $E_{accr}$  (1.07) are used in MG08, which helps to explain why most of the  
33 GCMs produce too frequent precipitation events but with too light precipitation intensity. The  
34 ratios of rain to cloud water mixing ratio at  $E_{accr}=1.07$  and  $E_{accr}=2.0$  are 0.063 and 0.142,  
35 respectively. from observations, further ~~proving~~ suggesting that the prescribed value of  
36  $E_{accr}=1.07$  used in MG08 is too small to simulate correct precipitation intensity. Both  $E_{auto}$  and  
37  $E_{accr}$  increase when the boundary layer becomes less stable, and the values are larger in  
38 precipitating clouds ( $CLWP > 75 \text{ gm}^{-2}$ ) than those in nonprecipitating clouds ( $CLWP < 75 \text{ gm}^{-2}$ ).  
39 Therefore, the selection of  $E_{auto}$  and  $E_{accr}$  values in GCMs should be regime- and resolution-  
40 dependent.



41

## 42 **1. Introduction**

43 Due to their vast areal coverage (Warren et al., 1986, 1988; Hahn and Warren, 2007) and  
44 strong radiative cooling effect (Hartmann et al., 1992; Chen et al., 2000), small changes in the  
45 coverage or thickness of marine boundary layer (MBL) clouds could change the radiative  
46 energy budget significantly (Hartmann and Short, 1980; Randall et al., 1984) or even offset the  
47 radiative effects produced by increasing greenhouse gases (Slingo, 1990). The lifetime of MBL  
48 clouds remains an issue in climate models (Yoo and Li, 2012; Jiang et al., 2012; Yoo et al.,  
49 2013; Stanfield et al., 2014) and represents one of the largest uncertainties in predicting future  
50 climate (Wielicki et al., 1995; Houghton et al., 2001; Bony and Dufresne, 2005).

51 MBL clouds frequently produce precipitation, mostly in the form of drizzle (Austin et al.,  
52 1995; Wood, 2005a; Leon et al., 2008; Wood, 2012). A significant amount of drizzle is  
53 evaporated before reaching the surface, for example, about ~76% over the Azores region in  
54 Northeast Atlantic (Wu et al., 2015), which provides another water vapour source for MBL  
55 clouds. Due to their pristine environment and their close vicinity to the surface, MBL clouds  
56 are especially sensitive to aerosol perturbations (Quaas et al., 2009; Kooperman et al., 2012).

57 ~~Most aerosol indirect effects are associated with precipitation suppression (Albrecht, 1989;~~  
58 ~~Ackerman et al., 2004; Lohmann and Feichter, 2005; Wood, 2007).~~ Thus, accurate prediction

59 of precipitation is essential in simulating the global energy budget and in constraining aerosol  
60 indirect effects in climate projections.

61 Due to the coarse spatial resolutions of the general circulation model (GCM) grid, many  
62 cloud processes cannot be adequately resolved and must be parameterized. For example, warm  
63 rain parameterizations in most GCMs treat the condensed water as either cloud or rain from the  
64 collision-coalescence process, which is partitioned into autoconversion and accretion sub-  
65 processes in model parameterizations (Kessler, 1969; Tripoli and Cotton, 1980; Beheng, 1994;  
66 Khairoutdinov and Kogan, 2000; Liu and Daum, 2004). Autoconversion represents the process  
67 that drizzle drops being formed through the condensation of cloud droplets and accretion  
68 represents the process where rain drops grow by the coalescence of drizzle-sized drops with  
69 cloud droplets. Autoconversion mainly accounts for precipitation initiation while accretion  
70 primarily contributes to precipitation intensity. Autoconversion is often parameterized as  
71 functions of cloud droplet number concentration ( $N_c$ ) and cloud water mixing ratio ( $q_c$ ), while  
72 accretion depends on both cloud and rain water mixing ratios ( $q_c$  and  $q_r$ ) (Kessler, 1969; Tripoli  
73 and Cotton, 1980; Beheng, 1994; Khairoutdinov and Kogan, 2000; Liu and Daum, 2004;  
74 Wood, 2005b). ~~All~~ The majority of previous studies suggested that these two processes as  
75 power law functions of cloud and precipitation properties (See section 2 for details).

76 In conventional GCMs, the lack of information on the sub-grid variances of cloud and  
77 precipitation leads to the unavoidable use of the grid-mean quantities  $\overline{N_c}$ ,  $\overline{q_c}$ , and  $\overline{q_r}$ , where

78 overbar denotes grid mean, same below) in calculating autoconversion and accretion rates.  
79 MBL cloud liquid water path (CLWP) distributions are often positive skewed (Wood and  
80 Hartmann, 2006; Dong et al., 2014a and 2014b), that is, the mean value is greater than mode  
81 value. Thus, the mean value only represents a relatively small portion of samples. Also, due to  
82 the nonlinear nature of the relationships, the two processes depend significantly on the sub-  
83 grid variability and co-variability of cloud and precipitation microphysical properties (Weber  
84 and Quass, 2012; Boutle et al., 2014). In some GCMs, sub-grid scale variability is often ignored  
85 or hard coded using constants to represent the variabilities under all meteorological conditions  
86 and across the entire globe (Pincus and Klein, 2000; Morrison and Gettleman, 2008; Lebrock  
87 et al., 2013). This could lead to systematic errors in precipitation rate simulations (Wood et al.,  
88 2002; Larson et al., 2011; Lebrock et al., 2013; Boutle et al., 2014; Song et al., 2018), where  
89 GCMs are found to produce too frequent but too light precipitation compared to observations  
90 (Zhang et al., 2002; Jess, 2010; Stephens et al., 2010; Nam and Quaas, 2012; Song et al., 2018).  
91 The bias is found to be smaller by using a probability density function (PDF) of cloud water to  
92 represent the sub-grid scale variability in autoconversion parameterization (Beheng, 1994;  
93 Zhang et al., 2002; Jess, 2010), or more complexly, by integrating the autoconversion rate over  
94 a joint PDF of liquid water potential temperature, ~~and vertical velocity~~, total water mixing ratio  
95 ~~and rain water mixing ratio~~ (Cheng and Xu, 2009).

96 Process rate enhancement factors ( $E$ ) are introduced when considering sub-grid scale  
97 variability in parameterizing grid-mean processes and they should be parameterized as  
98 functions of the PDFs of cloud and precipitation properties within a grid box (Morrison and  
99 Gettleman, 2008; Lebsock et al., 2013; Boutle et al., 2014). However, these values in some  
100 GCM parameterization schemes are prescribed as constants regardless of underlying surface  
101 or meteorological conditions (Xie and Zhang, 2015). Boutle et al. (2014) used aircraft in situ  
102 measurements and remote sensing techniques to develop a parameterization for cloud and rain,  
103 in which not only consider the sub-grid variabilities under different grid scales, but also  
104 consider the variation of cloud and rain fractions. The parameterization was found to reduce  
105 precipitation estimation bias significantly. Hill et al. (2015) modified this parameterization and  
106 developed a regime and cloud type dependent sub-grid parameterization, which was  
107 implemented to the Met Office Unified Model by Walters et al. (2017) and found that the  
108 radiation bias is reduced using the modified parameterization. Using ground-based  
109 observations and retrievals, Xie and Zhang (2015) proposed a scale-aware cloud  
110 inhomogeneity parameterization that they applied to the Community Earth System Model  
111 (CESM) and found that it can recognize spatial scales without manual tuning and can be applied  
112 to the entire globe. The inhomogeneity parameter is essential in calculating enhancement  
113 factors and affect the conversion rate from cloud to rain liquid. Xie and Zhang (2015), however,  
114 did not evaluate the validity of CESM simulations from their parameterization; the effect of  $N_c$

115 variability or the effect of covariance of cloud and rain on accretion process was not assessed.  
116 Most recently, Zhang et al. (2018) derived the sub-grid [distribution of](#) CLWP and  $N_c$  from the  
117 MODIS cloud product. They also studied the implication of the sub-grid cloud property  
118 variations for the autoconversion rate simulation, in particular the enhancement factor, in  
119 GCMs. For the first time, the enhancement factor due to the sub-grid variation of  $N_c$  is derived  
120 from satellite observation, and results reveal several regions downwind of biomass burning  
121 aerosols (e.g., Gulf of Guinea, East Coast of South Africa), air pollution (i.e., Eastern China  
122 Sea), and active volcanos (e.g., Kilauea Hawaii and Ambae Vanuatu), where the enhancement  
123 factor due to  $N_c$  is comparable, or even larger than that due to CLWP. However, one limitation  
124 of Zhang et al. (2018) is the use of passive remote sensing data only, which cannot distinguish  
125 cloud and rain water.

126 Dong et al. (2014a and 2014b) and Wu et al. (2015) reported MBL cloud and rain properties  
127 over the Azores and provided the possibility of calculating the enhancement factors using  
128 ground-based observations and retrievals. A joint retrieval method to estimate  $q_c$  and  $q_r$  profiles  
129 is proposed based on existing studies and is presented in Appendix A. Most of the calculations  
130 and analyses in this study is based on Morrison and Gettleman (2008, MG08 hereafter) scheme.  
131 The enhancement factors in several other schemes are also discussed and compared with the  
132 observational results and the approach in this study can be repeated for other microphysics  
133 schemes in GCMs. This manuscript is organized as follows: section 2 includes a summary of

134 the mathematical formulas from previous studies that can be used to calculate ~~grid-mean~~  
 135 ~~process~~-enhancement factors. Ground-based observations and retrievals are introduced in  
 136 Section 3. Section 4 presents results and discussions, followed by summary and conclusions in  
 137 Section 5. The retrieval method used in this study is in Appendix A.

## 138 2. Mathematical Background

139 Autoconversion and accretion rates in GCMs are usually parameterized as power law  
 140 equations (Tripoli and Cotton, 1980; Beheng, 1994; Khairoutdinov and Kogan, 2000; Liu and  
 141 Daum, 2004):

$$142 \left( \frac{\partial q_r}{\partial t} \right)_{auto} = A \bar{q}_c^{a1} \bar{N}_c^{a2}, \quad (1)$$

$$143 \left( \frac{\partial q_r}{\partial t} \right)_{accr} = B (\bar{q}_c \bar{q}_r)^b, \quad (2)$$

144 where  $A$ ,  $a1$ ,  $a2$ ,  $B$ , and  $b$  are coefficients in different schemes listed in Table 1. The  $\bar{q}_c$ ,  $\bar{q}_r$ ,  
 145 and  $\bar{N}_c$  are grid-mean cloud water mixing ratio, rain water mixing ratio, and droplet number  
 146 concentration, respectively. Because it is widely used in model parameterizations, the detailed  
 147 results from Khairoutdinov and Kogan (2000) parameterization that been used in MG08  
 148 scheme will be shown in Section 4 while a summary will be given for other schemes.

149 Ideally, the covariance between physical quantities should be considered in the calculation  
 150 of both processes. However,  $\bar{q}_c$  and  $\bar{N}_c$  in Eq. (1) are arguably not independently retrieved in  
 151 our retrieval method which will be introduced in this section and Appendix A. Thus we only

152 assess the individual roles of  $q_c$  and  $N_c$  sub-grid variations in determining autoconversion rate.  
 153  $q_c$  and  $q_r$ , on the other hand, are retrieved from two independent algorithms as shown in Dong  
 154 et al. (2014a and 2014b), Wu et al. (2015) and Appendix A, we will assess the effect of cloud  
 155 and rain property covariance on accretion rate calculations.

156 In the sub-grid scale, the PDFs of  $q_c$  and  $N_c$  are assumed to follow a gamma distribution  
 157 based on observational studies of optical depth in MBL clouds (Barker et al., 1996; Pincus et  
 158 al., 1999; Wood and Hartmann, 2006):

$$159 \quad P(x) = \frac{\alpha^\nu}{\Gamma(\nu)} x^{\nu-1} e^{-\alpha x}, \quad (3)$$

160 where  $x$  represents  $q_c$  or  $N_c$  with grid-mean quantity  $\bar{q}_c$  or  $\bar{N}_c$ , represented by  $\mu$ ,  $\alpha = \nu/\mu$  is the  
 161 scale parameter,  $\sigma^2$  is the relative variance of  $x$  (= variance divided by  $\mu^2$ ),  $\nu = 1/\sigma^2$  is the  
 162 shape parameter.  $\nu$  is an indicator of cloud field homogeneity, with large values representing  
 163 homogeneous and small values indicating inhomogeneous cloud field.

164 By integrating autoconversion rate, Eq. (1), over the grid-mean rate, Eq. (3), with respect  
 165 to sub-grid scale variation of  $q_c$  and  $N_c$ , the autoconversion rate can be expressed as:

$$166 \quad \left(\frac{\partial q_r}{\partial t}\right)_{auto} = A \mu_{q_c}^{a1} \mu_{N_c}^{a2} \frac{\Gamma(\nu+a)}{\Gamma(\nu)\nu^a}, \quad (4)$$

167 where  $a = a1$  or  $a2$ . Comparing Eq. (4) to Eq. (1), the autoconversion enhancement factor  
 168 ( $E_{auto}$ ) can be given with respect to  $q_c$  and  $N_c$ :

$$169 \quad E_{auto} = \frac{\Gamma(\nu+a)}{\Gamma(\nu)\nu^a}. \quad (5)$$

170 In addition to fitting the distributions of  $q_c$  and  $N_c$ , we also tried two other methods to  
 171 calculate  $E_{auto}$ . The first is to integrate Eq. (1) over the actual PDFs from observed or retrieved  
 172 parameters and the second is to fit a lognormal distribution for sub-grid variability like what  
 173 has been done in other studies (e.g., Lebsock et al., 2013; Larson and Griffin, 2013). It is found  
 174 that all three methods get similar results. In this study, we use a gamma distribution that is  
 175 consistent with MG08. Also note that, in the calculation of  $E_{auto}$  from  $\overline{N_c}$ , the negative exponent  
 176 (-1.79) may cause singularity problems in Eq. (5). When this situation occurs, we do direct  
 177 calculations by integrating the PDF of  $\overline{N_c}$  rather than using Eq. (5).

178 To account for the covariance of microphysical quantities in a model grid, it is difficult to  
 179 apply bivariate gamma distribution due to its complex nature. In this study, the bivariate  
 180 lognormal distribution of  $q_c$  and  $q_r$  is used (Lebsock et al., 2013; Boutle et al., 2014) and can  
 181 be written as:

$$\begin{aligned}
 182 \quad P(\overline{q_c}, \overline{q_r}) &= \frac{1}{2\pi\overline{q_c}\overline{q_r}\sigma_{q_c}\sigma_{q_r}\sqrt{1-\rho^2}} \exp \left\{ -\frac{1}{2} \frac{1}{1-\rho^2} \left[ \left( \frac{\ln\overline{q_c} - \mu_{q_c}}{\sigma_{q_c}} \right)^2 - 2\rho \left( \frac{\ln\overline{q_c} - \mu_{q_c}}{\sigma_{q_c}} \right) \left( \frac{\ln\overline{q_r} - \mu_{q_r}}{\sigma_{q_r}} \right) + \right. \right. \\
 183 \quad &\left. \left. \left( \frac{\ln\overline{q_r} - \mu_{q_r}}{\sigma_{q_r}} \right)^2 \right] \right\}, \tag{6}
 \end{aligned}$$

184 where  $\sigma$  is standard deviation and  $\rho$  is the correlation coefficient of  $q_c$  and  $q_r$ .

185 Similarly, by integrating the accretion rate in Eq. (2) from Eq. (6), we get the accretion  
 186 enhancement factor ( $E_{accr}$ ) of:



$$E_{accr} = \left(1 + \frac{1}{v_{qc}}\right)^{\frac{1.15^2 - 1.15}{2}} \left(1 + \frac{1}{v_{qr}}\right)^{\frac{1.15^2 - 1.15}{2}} \exp(\rho 1.15^2 \sqrt{\ln\left(1 + \frac{1}{v_{qc}}\right) \ln\left(1 + \frac{1}{v_{qr}}\right)}). \quad (7)$$

### 188 3. Ground-based observations and retrievals

189 The datasets used in this study were collected at the Department of Energy (DOE)  
 190 Atmospheric Radiation Measurement (ARM) Mobile Facility (AMF), which was deployed on  
 191 the northern coast of Graciosa Island (39.09°N, 28.03°W) from June 2009 to December 2010  
 192 (for more details, please refer to Rémillard et al., 2012; Dong et al., 2014a and Wood et al.,  
 193 2015). The detailed operational status of the remote sensing instruments on AMF was  
 194 summarized in Figure 1 of Rémillard et al. (2012) and discussed in Wood et al. (2015). The  
 195 ARM Eastern North Atlantic (ENA) site was established on the same island in 2013 and  
 196 provides long-term continuous observations.

197 The cloud-top heights ( $Z_{top}$ ) were determined from W-band ARM cloud radar (WACR)  
 198 reflectivity and only single-layered low-level clouds with  $Z_{top} \leq 3$  km are selected. Cloud-base  
 199 heights ( $Z_{base}$ ) were detected by a laser ceilometer (CEIL) and the cloud thickness was simply  
 200 the difference between cloud top and base heights. The cloud liquid water path (CLWP) was  
 201 retrieved from microwave radiometer (MWR) brightness temperatures measured at 23.8 and  
 202 31.4 GHz using a statistical retrieval method with an uncertainty of 20 g m<sup>-2</sup> for CLWP < 200  
 203 g m<sup>-2</sup>, and 10% for CLWP > 200 g m<sup>-2</sup> (Liljegren et al., 2001; Dong et al., 2000). Precipitating  
 204 status is identified through a combination of WACR reflectivity and  $Z_{base}$ . As in Wu et al.

205 (2015), we labelled the status of a specific time as “precipitating” if the WACR reflectivity  
206 below the cloud base exceeds -37 dBZ.

207 The ARM merged sounding data have a 1-min temporal and 20-m vertical resolution below  
208 3 km (Trojan, 2012). In this study, the merged sounding profiles are averaged to 5-min  
209 resolution. Pressure and temperature profiles are used to calculate air density ( $\rho_{air}$ ) profiles  
210 and to infer adiabatic cloud water content.

211 Cloud droplet number concentration ( $N_c$ ) is retrieved using the methods presented in Dong  
212 et al. (1998, 2014a and 2014b) and are assumed to be constant in a cloud layer. Vertical profiles  
213 of cloud and rain water content (CLWC and RLWC) are retrieved by combining WACR  
214 reflectivity, CEIL attenuated backscatter and by assuming adiabatic growth of cloud parcels.  
215 The detailed description is presented in Appendix A with the results from a selected case. The  
216 CLWC and RLWC values are transformed to  $q_c$  and  $q_r$  by dividing by air density (e.g.,  $q_c(z) =$   
217  $CLWC(z)/\rho_{air}(z)$ ).

218 The estimated uncertainties for the retrieved  $q_c$  and  $q_r$  are 30% and 18%, respectively (see  
219 Appendix A). We used the estimated uncertainties of  $q_r$  and  $q_c$  as inputs of Eqs. (4) and (7) to  
220 assess the uncertainties of  $E_{auto}$  and  $E_{accr}$ . For instance,  $(1 \pm 0.3)q_c$  are used in Eq. (4) and the  
221 mean differences are then used as the uncertainty of  $E_{auto}$ . Same method is used to estimate the  
222 uncertainty for  $E_{accr}$ .

223 The autoconversion and accretion parameterizations partitioned from the collision-  
224 coalescence process dominate at different levels in a cloud layer. Autoconversion dominates  
225 around cloud top where cloud droplets reach maximum by condensation and accretion is  
226 dominant at middle and lower parts of the cloud where rain drops sediment and continue to  
227 grow by collecting cloud droplets. Complying with the physical processes, we estimate  
228 autoconversion and accretion rates at different levels of a cloud layer in this study. The  
229 averaged  $q_c$  within the top five range gates (~215 m thick) are used to calculate  $E_{auto}$ . To  
230 calculate  $E_{accr}$ , we use the averaged  $q_c$  and  $q_r$  within five range gates around the maximum  
231 radar reflectivity. If the maximum radar reflectivity appears at the cloud base, then five range  
232 gates above the cloud base are used.

233 The ARM merged sounding data are also used to calculate lower tropospheric stability  
234 ( $LTS = \theta_{700\text{ hPa}} - \theta_{1000\text{ hPa}}$ ), which is used to infer the boundary layer stability. In this study,  
235 unstable and stable boundary layers are defined as LTS less than 13.5 K and greater than 18 K,  
236 respectively, and environment with an LTS between 13.5 K and 18 K is defined as mid-stable  
237 (Wang et al. 2012; Bai et al. 2018). Enhancement factors in different boundary layers are  
238 summarized in Section 4.2 and may be used as references for model simulations. Further, two  
239 regimes are classified: CLWP greater than 75 g m<sup>-2</sup> as precipitating and CLWP less than 75 g  
240 m<sup>-2</sup> as nonprecipitating (Rémillard et al., 2012).

241 To evaluate the dependence of autoconversion and accretion rates on sub-grid variabilities  
242 for different model spatial resolutions, an averaged wind speed within a cloud layer was  
243 extracted from merged sounding and used in sampling observations over certain periods to  
244 mimic different grid sizes in GCMs. For example, two hours of observations corresponds to a  
245 72-km horizontal equivalent grid box if mean in-cloud wind speed is  $10 \text{ m s}^{-1}$  horizontal wind  
246 and if the wind speed is  $5 \text{ m s}^{-1}$ , four hours of observations is needed to mimic the same  
247 horizontal equivalent grid. We used six horizontal equivalent grid sizes (30-, 60-, 90-, 120-,  
248 150-, and 180-km) and mainly show the results from 60-km and 180-km horizontal equivalent  
249 grid sizes in Section 4. For convenience, we refer ‘equivalent size’ as ‘horizontal equivalent  
250 grid size’ from now on.

Formatted: Font: (Asian) +Body Asian (SimSun), (Asian) Chinese (PRC), (Other) English (United States)

## 251 4. Results and discussions

252 In this section, we first show the data and methods using a selected case, followed by  
253 statistical analysis based on 19 months of data and multiple time-intervals.

### 254 4.1 Case study

255 The selected case occurred on July 27, 2010 (Figure 1a) at the Azores. This case was  
256 characterized by a long time of non-precipitating or light drizzling cloud development (00:00-  
257 14:00 UTC) before intense drizzling occurred (14:00-20:00 UTC). Wu et al. (2017) studied  
258 this case in detail to demonstrate the effect of wind shear on drizzle initiation. Here, we choose  
259 two periods corresponding to a 180-km equivalent size-grid and having similar mean  $q_c$  near

260 cloud top:  $0.28 \text{ g kg}^{-1}$  for period c and  $0.26 \text{ g kg}^{-1}$  for period d but with different distributions  
261 (Figures 1c and 1d). The PDFs of  $q_c$  are then fitted using gamma distributions to get shape  
262 parameters ( $\nu$ ) as shown in Figures 1c and 1d. Smaller  $\nu$  is usually associated with a more  
263 inhomogeneous cloud field, which allows more rapid drizzle production and more efficient  
264 liquid transformation from cloud to rain (Xie and Zhang, 2015) in regions that satisfy  
265 precipitation criteria, which is usually controlled using threshold  $q_r$ , droplet size or relative  
266 humidity (Kessler, 1969; Liu and Daum, 2004). The period d has a wider  $q_c$  distribution than  
267 the period c, resulting in a smaller  $\nu$  and thus larger  $E_{auto}$ . Using the fitted  $\nu$ , the  $E_{auto}$  from  $q_c$   
268 is calculated from Eq. (5) and the period d is larger than the period c (1.80 vs. 1.33). The  $E_{auto}$   
269 values for the periods d and c can also be calculated from  $N_c$  using the same procedure as  $q_c$   
270 with a similar result (2.1 vs. 1.51). The  $E_{accr}$  values for the periods d and c can be calculated  
271 from the covariance of  $q_c$  and  $q_r$  and Eq. (7). Not surprisingly, the period d has larger  $E_{accr}$  than  
272 the period c. The combination of larger  $E_{auto}$  and  $E_{accr}$  in the period d contributes to the rapid  
273 drizzle production and high rain rate as seen from WACR reflectivity and  $q_r$  [in Figure A1](#).

274 It is important to understand the physical meaning of enhancement factors in precipitation  
275 parameterization. For example, if we assume two scenarios for  $q_c$  with a model grid having the  
276 same mean values but different distributions: (1) The distribution is extremely homogeneous,  
277 there will be no sub-grid variability because the cloud has the same chance to precipitate and  
278 the enhancement factors would be unity (this is true for arbitrary grid-mean  $q_c$  amount as well).

279 (2) The cloud field gets more and more inhomogeneous with a broad range of  $q_c$  within the  
280 model grid box, which results in a greater enhancement factor and increases the possibility of  
281 precipitation. That is, a large enhancement factor can make the part of the cloud with higher  $q_c$   
282 within the grid box become more efficient in generating precipitation, rather than the entire  
283 model grid.

284 Using the LWP retrieved from the Moderate Resolution Imaging Spectroradiometer  
285 (MODIS) as an indicator of cloud inhomogeneous, Wood and Hartmann (2006) found that  
286 when clouds become more inhomogeneous, cloud fraction decreases, and open cells become  
287 dominant with stronger drizzling process (Comstock et al., 2007). The relationship between  
288 reduced homogeneity and stronger precipitation intensity is found in this study, which is similar  
289 to the findings in other studies (e.g., Wood and Hartmann, 2006, Comstock et., 2007, Barker  
290 et al., 1996; Pincus et al., 1999).

291 It is clear that  $q_c$  and  $N_c$  in Figure 1b are correlated with each other. In addition to their  
292 natural relationships,  $q_c$  and  $N_c$  in our retrieval method are also correlated (Dong et al., 2014a  
293 and 2014b). Thus, the effect of  $q_c$  and  $N_c$  covariance on  $E_{auto}$  is not included in this study. In  
294 Figures 1c and 1d, the results are calculated using equivalent size-model-grid of 180-km for the  
295 selected case on 27 July 2010. In Section 4.2, we will use these approaches to calculate their  
296 statistical results for multiple equivalent-grid sizes using the 19-month ARM ground-based  
297 observations and retrievals.

## 298 4.2 Statistical result

299 For a specific equivalent grid-size, e.g. 60-km, we estimate the shape parameter ( $\nu$ ) and  
300 calculate  $E_{auto}$  through Eqns. (5) and (7). The PDFs of  $E_{auto}$  for both 60-km and 180-km  
301 equivalent grids-sizes are shown in Figures 2a-2d. The distributions of  $E_{auto}$  values calculated  
302 from  $q_c$  with 60-km and 180-km equivalent grid-sizes (Figures 2a and 2b) are different to each  
303 other (2.79 vs. 3.3). The calculated  $E_{auto}$  values range from 1 to 10, and most are less than 4.  
304 The average value for the 60-km equivalent sizegrid (2.79) is smaller than that for the 180-km  
305 equivalent sizegrid (3.2), indicating a possible dependence of  $E_{auto}$  on model grid size. Because  
306 drizzle-sized drops are primarily resulted from the autoconversion, we investigate the  
307 relationship between  $E_{auto}$  and precipitation frequency, which is defined as the average  
308 percentage of drizzling occurrence based on radar reflectivity below the cloud base. Given the  
309 average LWP at Azores from Dong et al. (2014b, 109-140 g m<sup>-2</sup>), the precipitation frequency  
310 (black lines in Figures 2a and 2b) agrees well with those from Kubar et al. (2009, 0.1-0.7 from  
311 their Figure 11). The precipitation frequency within each bin shows an increasing trend for  
312  $E_{auto}$  from 0 to 4-6, then oscillates ~~around a relative constant~~ when  $E_{auto} > 6$ , indicating that in  
313 precipitation initiation process,  $E_{auto}$  keeps increasing to a certain value ( $\sim 6$ ) until the  
314 precipitation frequency reaches a near-steady state. Larger  $E_{auto}$  values do not necessarily result  
315 in higher precipitation frequency but instead may produce more drizzle-sized drops from  
316 autoconversion process when the cloud is precipitating.

317 The PDFs of  $E_{auto}$  calculated from  $N_c$  also share similar patterns of positive skewness and  
318 peaks at  $\sim 1.5$ - $2.0$  for the 60-km and 180-km equivalent grid-sizes (Figures 2c and 2d). Although  
319 the average values are close to their  $q_c$  counterparts (2.54 vs. 2.79 for 60-km and 3.45 vs. 3.2  
320 for 180-km), the difference in  $E_{auto}$  between 60-km and 180-km equivalent grid-sizes becomes  
321 large. The precipitation frequencies within each bin are nearly constant or slightly decrease,  
322 which are different to their  $q_c$  counterparts shown in Figures 2a and 2b. This suggests  
323 complicated effects of droplet number concentration on precipitation initiation and warrants  
324 more explorations of aerosol-cloud-precipitation interactions. ~~This is very intriguing result,~~  
325 ~~which suggests the existence of significant sub-grid variation of  $N_c$  and this variation can~~  
326 ~~significantly influence the warm rain process.~~ As mentioned in Section 2,  $q_c$  and  $N_c$  are also  
327 fitted using lognormal distributions to calculate  $E_{auto}$ , those are close to the results in Figure 2  
328 (not shown here) with average values of 3.28 and 3.84, respectively, for 60-km and 180-km  
329 equivalent grid-sizes. Because the  $E_{auto}$  values calculated from  $q_c$  and  $N_c$  are close to each  
330 other, we will focus on analyzing the results from  $q_c$  only for simplicity and clarity. The effect  
331 of  $q_c$  and  $N_c$  covariance, as stated in Section 4.1, is not presented in this study due to the intrinsic  
332 correlation in the retrieval (Dong et al., 2014a and 2014b and Appendix A of this study).

333 The covariance of  $q_c$  and  $q_r$  is included in calculating  $E_{accr}$  and the results are shown in  
334 Figures 2e and 2f. The calculated  $E_{accr}$  values range from 1 to 4 with mean values of 1.62 and  
335 1.76 for 60-km and 180-km equivalent grid-sizes, respectively. These two mean values are



336 much greater than the prescribed value used in MG08 (1.07). Since accretion is dominant at  
337 middle and lower parts of the cloud where rain drops sediment and continue to grow by  
338 collecting cloud droplets, we superimpose the ratio of  $q_r$  to  $q_c$  within each bin (black lines in  
339 Figures 2e and 2f) to represent the portion of rain water in the cloud layer. In both panels, the  
340 ratios are less than 15%, which means that  $q_r$  can be one order of magnitude smaller than  $q_c$ .  
341 The differences in magnitude are consistent with previous CloudSat and aircraft results (e.g.,  
342 Boutle et al., 2014). This ratio increases from  $E_{accr}=0$  to  $\sim 2$ , and then decreases, suggesting a  
343 possible optimal state for the collision-coalescence process to achieve maximum efficiency for  
344 converting cloud water into rain water at  $E_{accr}=2$ . In other words, the conversion efficiency  
345 cannot be infinitely increased with  $E_{accr}$  under available cloud water. The ratio of  $q_r$  to  $q_c$   
346 increases from  $E_{accr}=1.07$  (0.063) to  $E_{accr}=2.0$  (0.142), indicating that the fraction of rain water  
347 in total water using the prescribed  $E_{accr}$  is too low. This ratio could be increased significantly  
348 using a large  $E_{accr}$  value, therefore increasing precipitation intensity in the models. This further  
349 proves that the prescribed value of  $E_{accr}=1.07$  used in MG08 is too small to correctly simulate  
350 precipitation intensity in the models. Therefore, similar to the conclusions in Lebsack et al.  
351 (2013) and Boutle et al. (2014), we suggest increasing  $E_{accr}$  from 1.07 to 1.5-2.0 in GCMs.

352 To illustrate the impact of using prescribed enhancement factors, autoconversion and  
353 accretion rates are calculated using the prescribed values (e.g., 3.2 for  $E_{auto}$  and 1.07 for  $E_{accr}$ ,  
354 MG08; Xie and Zhang, 2015) and the newly calculated ones in Figure 2 that use observations

355 and retrievals. Figure 3 shows the joint density of autoconversion (Figures 3a and 3b) and  
356 accretion rates (Figures 3c and 3d) from observations (x-axis) and model parameterizations (y-  
357 axis) for 60-km and 180-km equivalent grid-sizes. Despite the spread, the peaks of the joint  
358 density of autoconversion rate appear slightly above the one-to-one line especially for the 60-  
359 km equivalent size, suggesting that cloud droplets in the model are more easily to be converted  
360 into drizzle/rain drops than observations. On the other hand, the peaks of accretion rate appear  
361 slightly below the one-to-one line which indicates that simulated precipitation intensities are  
362 lower than observed ones. The magnitudes of the two rates are consistent with Khairoutdinov  
363 and Kogan (2000), Liu and Daum (2004), and Wood (2005b).

364 Compared to the observations, the precipitation in GCMs occurs at higher frequencies with  
365 lower intensities, which might explain why the total precipitation amounts are close to surface  
366 measurements over an entire grid box. This ‘promising’ result, however, fails to simulate  
367 precipitation on the right scale and cannot capture the correct rain water amount, thus providing  
368 limited information in estimating rain water evaporation and air-sea energy exchange.

369 Clouds in an unstable boundary layer have a better chance of getting moisture supply from  
370 the surface by upward motion than clouds in a stable boundary layer. Precipitation frequencies  
371 are thus different in these two boundary layer regimes. For example, clouds in a relatively  
372 unstable boundary layer more easily produce drizzle than those in a stable boundary layer (Wu  
373 et al., 2017). Provided the same boundary layer condition, CLWP is an important factor in

374 determining the precipitation status of clouds. At the Azores, precipitating clouds are more  
375 likely to have CLWP greater than  $75 \text{ g m}^{-2}$  than their nonprecipitating counterparts (Rémillard  
376 et al., 2012). To further investigate what conditions and parameters can significantly influence  
377 the enhancement factors, we classify low-level clouds according to their boundary layer  
378 conditions and CLWPs.

379 The averaged  $E_{auto}$  and  $E_{accr}$  values for each category are listed in Table 2. Both  $E_{auto}$  and  
380  $E_{accr}$  increase when the boundary layer becomes less stable, and these values become larger in  
381 precipitating clouds ( $CLWP > 75 \text{ gm}^{-2}$ ) than those in nonprecipitating clouds ( $CLWP < 75 \text{ gm}^{-2}$ ).  
382 In real applications, autoconversion process only occurs when  $q_c$  or cloud droplet size reaches  
383 a certain threshold (e.g., Kessler, 1969 and Liu and Daum, 2004). Thus, it will not affect model  
384 simulations if a valid  $E_{auto}$  is assigned to Eq. (1) in a nonprecipitating cloud. The  $E_{auto}$  values  
385 in both stable and mid-stable boundary layer conditions are smaller than the prescribed value  
386 of 3.2, while the values in unstable boundary layers are significantly larger than 3.2 regardless  
387 of if they are precipitating or not. All  $E_{accr}$  values are greater than the constant of 1.07. The  
388  $E_{auto}$  values in Table 2 range from 2.32 to 6.94 and the  $E_{accr}$  values vary from 1.42 to 1.86,  
389 depending on different boundary layer conditions and CLWPs. Therefore, as suggested by Hill  
390 et al. (2015), the selection of  $E_{auto}$  and  $E_{accr}$  values in GCMs should be regime-dependent.

391 To properly parameterize sub-grid variabilities, the approaches by Hill et al. (2015) and  
392 Walters et al. (2017) can be adopted. To use MG08 and other parameterizations in GCMs as

393 listed in Table 1, proper adjustments can be made according to the model grid size, boundary  
394 layer conditions, and precipitating status. As stated in the methodology, we used a variety of  
395 ~~equivalent model grid~~-sized. Figure 4 demonstrates the dependence of both enhancement  
396 factors on different model grid sizes. The  $E_{auto}$  values (red line) increase from 1.97 at an  
397 ~~equivalent grid box size~~ of 30×30 km to 3.15 at an ~~equivalent grid box size~~ of 120×120 km,  
398 which are 38.4% and 2% percent lower than the prescribed value (3.2, upper dashed line). After  
399 that, the  $E_{auto}$  values remain relatively constant of ~3.18 when the ~~equivalent model grid size~~  
400 is 180 km, which is close to the prescribed value of 3.2 used in MG08. This result indicates  
401 that the prescribed value in MG08 represents well in large grid sizes in GCMs. The  $E_{accr}$  values  
402 (blue line) increase from 1.53 at an ~~equivalent grid box size~~ of 30×30 km to 1.76 at an ~~equivalent~~  
403 ~~grid box size~~ of 180×180 km, those are 43% and 64%, respectively, larger than the prescribed  
404 value (1.07, lower dashed line). The shaded areas represent the uncertainties of  $E_{auto}$  and  $E_{accr}$   
405 associated with the uncertainties of the retrieved  $q_c$  and  $q_r$ . When ~~model equivalent grid size~~  
406 increases, the uncertainties slightly decrease. The prescribed  $E_{auto}$  is close to the upper  
407 boundary of uncertainties except for the 30-km ~~equivalent grid size~~, while the prescribed  $E_{accr}$   
408 is significantly lower than the lower boundary.

409 It is noted that  $E_{auto}$  and  $E_{accr}$  depart from their prescribed values at opposite directions as  
410 ~~the equivalent model grid size~~ increases. For models with finer resolutions (e.g., 30-km), both  
411  $E_{auto}$  and  $E_{accr}$  are significantly different from the prescribed values, which can partially explain

412 the issue of ‘too frequent’ and ‘too light’ precipitation. Under both conditions, the accuracy of  
413 precipitation estimation is degraded. For models with coarser resolutions (e.g., 180-km),  
414 average  $E_{auto}$  is exactly 3.2 while  $E_{accr}$  is much larger than 1.07 when compared to finer  
415 resolution simulations. In such situations, the simulated precipitation will be dominated by the  
416 ‘too light’ problem, in addition to regime-dependent (Table 2) and as in Xie and Zhang (2015),  
417  $E_{auto}$  and  $E_{accr}$  should be also scale-dependent.

418 Also note that the location ~~we choose to collect~~of ground-based observations and retrievals  
419 ~~used in this study~~ is on the remote ocean where the MBL clouds mainly form in a relatively  
420 stable boundary layer and are characterized by high precipitation frequency. Even in such  
421 environments, however, the GCMs overestimate the precipitation frequency (Ahlgren and  
422 Forbes, 2014).

423 To further investigate how enhancement factors affect precipitation simulations, we use  
424  $E_{auto}$  as a fixed value of 3.2 in Eq. (4), and then calculate the  $q_c$  needed for models to reach the  
425 same autoconversion rate as observations. The  $q_c$  differences between models and observations  
426 are then calculated, which represent the  $q_c$  adjustment in models to get a realistic  
427 autoconversion rate in the simulations. Similar to Figure 1, the PDFs of  $q_c$  differences (model  
428 – observation) are plotted in Figures 5a and 5b for 60-km and 180-km ~~equivalent grid~~-sized.  
429 Figure 5c shows the average percentages of model  $q_c$  adjustments for different ~~equivalent~~  
430 ~~model grid~~-sized. The mode and average values for 30-km ~~equivalent grid size~~ is negative,

431 suggesting that models need to simulate lower  $q_c$  in general to get reasonable autoconversion  
432 rates. Lower  $q_c$  values are usually associated with smaller  $E_{auto}$  values that induce lower  
433 simulated precipitation frequency. On average, the percentage of  $q_c$  adjustments decrease with  
434 increasing equivalent model grid size. For example, the adjustments for finer resolutions (e.g.,  
435 30-60 km) can be ~20% of the  $q_c$ , whereas adjustments in coarse resolution models (e.g., 120  
436 – 180 km) are relatively small because the prescribed  $E_{auto}$  (=3.2) is close to the observed ones  
437 (Figure 4) and when equivalent model grid-size is 180-km, no adjustment is needed. The  
438 adjustment method presented in Figure 5, however, may change cloud water substantially and  
439 may cause a variety of subsequent issues, such as altering cloud radiative effects and disrupting  
440 the hydrological cycle. The assessment in Figure 5 only provides a reference to the equivalent  
441 effect on cloud water by using the prescribed  $E_{auto}$  value as compared to those from  
442 observations.

443 All above discussions are based on the prescribed  $E_{auto}$  and  $E_{accr}$  values (3.2 and 1.07) in  
444 MG08. Whereas there are quite a few parameterizations that have been published so far. In this  
445 study, we list  $E_{auto}$  and  $E_{accr}$  for three other widely used parameterization schemes in Table 3,  
446 which are given only for 60-km and 180-km equivalent grid-sizes. The values of the exponent  
447 in each scheme directly affect the values of the enhancement factors. For example, the scheme  
448 in Beheng (1994) has highest degree of nonlinearity and hence has the largest enhancement  
449 factors. The scheme in Liu and Daum (2004) is very similar to the scheme in Khairoutdinov

450 and Kogan (2000) because both schemes have a physically realistic dependence on cloud water  
451 content and number concentration (Wood, 2005b). For a detailed overview and discussion of  
452 various existing parameterizations, please refer to Liu and Daum (2004), Liu et al. (2006a), Liu  
453 et al. (2004b), Wood (2005b) and Michibata and Takemura (2015). A physical based  
454 autoconversion parameterization was developed by Lee and Baik (2017) in which the scheme  
455 was derived by solving stochastic collection equation with an approximated collection kernel  
456 that is constructed using the terminal velocity of cloud droplets and the collision efficiency  
457 obtained from a particle trajectory model. Due to the greatly increased complexity of their  
458 equation, we do not attempt to calculate  $E_{auto}$  here but should be examined in future studies due  
459 to the physics feasibility of the Lee and Baik (2017) scheme.

460

## 461 **5. Summary**

462 To better understand the influence of sub-grid cloud variations on the warm-rain process  
463 simulations in GCMs, we investigated the warm-rain parameterizations of autoconversion  
464 ( $E_{auto}$ ) and accretion ( $E_{accr}$ ) enhancement factors in MG08. These two factors represent the  
465 effects of sub-grid cloud and precipitation variabilities when parameterizing autoconversion  
466 and accretion rates as functions of grid-mean quantities.  $E_{auto}$  and  $E_{accr}$  are prescribed as 3.2  
467 and 1.07, respectively, in the widely used MG08 scheme. To assess the dependence of the two  
468 parameters on sub-grid scale variabilities, we used ground-based observations and retrievals

469 collected at the DOE ARM Azores site to reconstruct the two enhancement factors in different  
470 ~~equivalent model grid~~ sizes.

471 From the retrieved  $q_c$  and  $q_r$  profiles, the averaged  $q_c$  within the top five range gates are  
472 used to calculate  $E_{auto}$  and the averaged  $q_c$  and  $q_r$  within five range gates around maximum  
473 reflectivity are used to calculate  $E_{accr}$ . The calculated  $E_{auto}$  values from observations and  
474 retrievals increase from 1.96 at ~~an equivalent sizegrid box~~ of ~~30×30~~ km to 3.18~~5~~ at ~~an~~  
475 ~~equivalent sizegrid box~~ of ~~1520×120~~ km. These values are 38% and ~~20.625~~% lower than the  
476 prescribed value of 3.2. The prescribed value in MG08 represents well in large grid sizes in  
477 GCMs ~~(e.g., 180<sup>2</sup> km<sup>2</sup> grid)~~. On the other hand, the  $E_{accr}$  values increase from 1.53 at ~~an~~  
478 ~~equivalent sizegrid box~~ of ~~30×30~~ km to 1.76 at ~~an equivalent sizegrid box~~ of ~~180×180~~ km,  
479 which are 43% and 64% higher than the prescribed value (1.07). The higher  $E_{auto}$  and lower  
480  $E_{accr}$  prescribed in GCMs help to explain the issue of too frequent precipitation events with too  
481 light precipitation intensity. The ratios of rain to cloud liquid water increase with increasing  
482  $E_{accr}$  from 0 to 2, and then decrease after that, suggesting a possible optimal state for the  
483 collision-coalescence process to achieve maximum efficiency for converting cloud water into  
484 rain water at  $E_{accr}=2$ . The ratios of  $q_r$  to  $q_c$  at  $E_{accr}=1.07$  and  $E_{accr}=2.0$  are 0.063 and 0.142,  
485 further proving that the prescribed value of  $E_{accr}=1.07$  is too small to simulate correct  
486 precipitation intensity in models.

Formatted: Superscript

Formatted: Superscript



487 To further investigate what conditions and parameters can significantly influence the  
488 enhancement factors, we classified low-level clouds according to their boundary layer  
489 conditions and CLWPs. Both  $E_{auto}$  and  $E_{accr}$  increase when the boundary layer conditions  
490 become less stable, and the values are larger in precipitating clouds ( $CLWP > 75 \text{ gm}^{-2}$ ) than  
491 those in nonprecipitating clouds ( $CLWP < 75 \text{ gm}^{-2}$ ). The  $E_{auto}$  values in both stable and mid-stable  
492 boundary layer conditions are smaller than the prescribed value of 3.2, while those in unstable  
493 boundary layers conditions are significantly larger than 3.2 regardless of whether or not the  
494 cloud is precipitating (Table 2). All  $E_{accr}$  values are greater than the prescribed value of 1.07.  
495 Therefore, the selection of  $E_{auto}$  and  $E_{accr}$  values in GCMs should be regime-dependent, which  
496 also has been suggested by Hill et al. (2015) and Walters et al. (2017).

497 This study, however, did not include the effect of uncertainties in GCM simulated cloud  
498 and precipitation properties on sub-grid scale variations. For example, we did not consider the  
499 behavior of the two enhancement factors under different aerosol regimes, a condition which  
500 may affect precipitation formation process. The effect of aerosol-cloud-precipitation-  
501 interactions on cloud and precipitation sub-grid variabilities may be of comparable importance  
502 to meteorological regimes and precipitation status and deserves a further study. Other than the  
503 large-scale dynamics, e.g., LTS in this study, upward/downward motion in sub-grid scale may  
504 also modify cloud and precipitation development and affect the calculations of enhancement  
505 factors. The investigation of the dependence of  $E_{auto}$  and  $E_{accr}$  on aerosol type and concentration

506 as well as on vertical velocity would be a natural extension and complement of current study.  
507 In addition, other factors may also affect precipitation frequency and intensity even under the  
508 same aerosol regimes and even if the clouds have similar cloud water contents. Wind shear, for  
509 example as presented in Wu et al. (2017), is an external variable that can affect precipitation  
510 formation. Further studies are needed to evaluate the role of the covariance of  $q_c$  and  $N_c$  in sub-  
511 grid scales on  $E_{auto}$  determinations, which is beyond the scope of this study and requires  
512 independent retrieval techniques.

513

#### 514 **Appendix A: Joint cloud and rain LWC profile estimation**

515 If a time step is identified as non-precipitating, the cloud liquid water content (CLWC)  
516 profile is retrieved using Frisch et al. (1995) and Dong et al. (1998, 2014a and 2014b). The  
517 retrieved CLWC is proportional to radar reflectivity.

518 If a time step is identified as precipitating (maximum reflectivity below cloud base  
519 exceeds -37 dBZ), CLWC profile is first inferred from temperature and pressure in merged  
520 sounding by assuming adiabatic growth. Marine stratocumulus is close to adiabatic (Albrecht  
521 et al. 1990) and was used in cloud property retrievals in literature (e.g., Rémillard et al., 2013).  
522 In this study, we use the information from rain properties near cloud base to further constrain  
523 the adiabatic CLWC ( $CLWC_{adiabatic}$ ).

524 Adopting the method of O'Connor et al. (2005), Wu et al. (2015) retrieved rain properties  
 525 below cloud base (CB) for the same period as in this study. In Wu et al. (2015), rain drop size  
 526 (median diameter,  $D_0$ ), shape parameter ( $\mu$ ), and normalized rain droplet number concentration  
 527 ( $N_W$ ) are retrieved for the assumed rain particle size distribution (PSD):

$$528 \quad n_r(D) = N_W f(\mu) \left(\frac{D}{D_0}\right)^\mu \exp\left[-\frac{(3.67+\mu)D}{D_0}\right] \quad (\text{A1})$$

529 To infer rain properties above cloud base, we adopt the assumption in Fielding et al. (2015)  
 530 that  $N_W$  increases from below CB to within the cloud. This assumption is consistent with the *in*  
 531 *situ* measurement in Wood (2005a). Similar as Fielding et al. (2015), we use constant  $N_W$  within  
 532 cloud if the vertical gradient of  $N_W$  is negative~~decrease with height~~ below CB. The  $\mu$  within  
 533 cloud is treated as constant and is taken as the averaged value from four range gates below CB.  
 534 Another assumption in the retrieval is that the evaporation of rain drops is negligible from one  
 535 range gate above CB to one range gate below CB thus we assume rain drop size is the same at  
 536 the range gate below and above CB.

537 With the above information, we can calculate the reflectivity contributed by rain at the first  
 538 range gate above CB ( $Z_{dr}(1)$ ) and the cloud reflectivity ( $Z_c(1)$ ) is then  $Z_c(1) = Z(1) - Z_{dr}(1)$ ,  
 539 where  $Z(1)$  is WACR measured reflectivity at first range gate above CB. Using cloud droplet  
 540 number concentration ( $N_c$ ) from Dong et al. (2014a and 2014b), CLWC at the first range gate  
 541 above CB can be calculated through

Formatted: Font: Italic

Formatted: Font: Italic

$$Z_c(1) = 2^6 \int_0^\infty n_c(r) r^6 dr = \frac{36}{\pi^2 \rho_w^2} \frac{CLWC(1)_{reflectivity}^2}{N_c} \exp(9\sigma_x^2)$$

543 (A2.1)

$$544 \quad CLWC(1)_{reflectivity} = \sqrt{\frac{Z_c(1) \pi^2 \rho_w^2 N_c}{36 \exp(9\sigma_x^2)}} \quad (A2.2)$$

545 Where  $\rho_w$  is liquid water density  $n_c(r)$  is lognormal distribution of cloud PSD with  
 546 logarithmic width  $\sigma_x$  which is set to a constant value of 0.38 (Miles et al., 2000). Geoffroy et  
 547 al. (2010) suggested that  $\sigma_x$  increases with the length scale and Witte et al. (2018) showed that  
 548  $\sigma_x$  also dependent on the choice instrumentation. The variations of  $\sigma_x$  should be reflected in  
 549 the retrieval by using different  $\sigma_x$  values with time. However, no aircraft measurements were  
 550 available during CAP-MBL to provide  $\sigma_x$  over the Azores region. The inclusion of solving  $\sigma_x$   
 551 in the retrieval adds another degree of freedom to the equations and complicates the problem  
 552 considerably. In this study,  $\sigma_x$  is set to a constant value of 0.38 from Miles et al. (2000), which  
 553 is a statistical value from aircraft measurements of marine low-level clouds.  ~~$\rho_w$  is liquid water~~  
 554 ~~density.~~

555 We then compare the  $CLWC_{adiabatic}$  and the one calculated from  $CLWC_{reflectivity}$  at the  
 556 first range gate above CB. A scale parameter ( $s$ ) is defined as  $s = \frac{CLWC_{reflectivity}(1)}{CLWC_{adiabatic}(1)}$  and the  
 557 entire profile of  $CLWC_{adiabatic}$  is multiplied by  $s$  to correct the bias from cloud sub-  
 558 adiabaticity. Reflectivity profile from cloud is then calculated from Eq. (A2.1) using the  
 559 updated  $CLWC_{adiabatic}$  and the remaining reflectivity profile from WACR observation is

560 regarded as rain contribution. Rain particle size can then be calculated given that  $N_W$  and  $\mu$  are  
561 known and rain liquid water content (RLWC) can be estimated.

562 There are two constrains used in the retrieval. One is that the summation of cloud and rain  
563 liquid water path (CLWP and RLWP) must be equal to the LWP from microwave radiometer  
564 observation. Another is that rain drop size ( $D_0$ ) near cloud top must be equal or greater than 50  
565  $\mu m$  and if  $D_0$  is less than 50  $\mu m$ , we decrease  $N_W$  for the entire rain profile within cloud and  
566 repeat the calculation until the 50  $\mu m$  criteria is satisfied.

567 It is difficult to quantitatively estimate the retrieval uncertainties without aircraft in situ  
568 measurements. For the proposed retrieval method, 18% should be used as uncertainty for  
569 RLWC from rain properties in Wu et al. (2015) and 30% for CLWC from cloud properties in  
570 Dong et al. (2014a and 2014b). The actual uncertainty depends on the accuracy of merged  
571 sounding data, the detectability of WACR near cloud base and the effect of entrainment on  
572 cloud adiabaticity during precipitating. In the recent aircraft field campaign, the Aerosol and  
573 Cloud Experiments in Eastern North Atlantic (ACE-ENA) was conducted during 2017-2018  
574 with a total of 39 flights over the Azores, near the ARM ENA site on Graciosa Island. These  
575 aircraft in situ measurements will be used to validate the ground-based retrievals and  
576 quantitatively estimate their uncertainties in the future.

577 Figure A1 shows an example of the retrieval results. The merged sounding, ceilometer,  
578 microwave radiometer, WACR and ceilometer are used in the retrieval. Whenever one or more

579 instruments are not reliable, that time step is skipped, and this results in the gaps in the CLWC  
580 and RLWC as shown in Figures A1(b) and A1(c). When the cloud is classified as  
581 nonprecipitating, no RLWC will be retrieved as well. Using air density ( $\rho_{air}$ ) profiles  
582 calculated from temperature and pressure in merged sounding, mixing ratio ( $q$ ) can be  
583 calculated from LWC using  $q(z) = LWC(z)/\rho_{air}(z)$ .

#### 584 **Acknowledgements**

585 The ground-based measurements were obtained from the Atmospheric Radiation Measurement  
586 (ARM) Program sponsored by the U.S. Department of Energy (DOE) Office of Energy  
587 Research, Office of Health and Environmental Research, and Environmental Sciences  
588 Division. The data can be downloaded from <http://www.archive.arm.gov/>. This research was  
589 supported by the DOE CESM project under grant DE-SC0014641 at the University of Arizona  
590 through subaward from University of Maryland at Baltimore County, and the NSF project  
591 under grant AGS-1700728 at University of Arizona. The authors thank Dr. Yangang Liu at  
592 Brookhaven National Laboratory for insightful comments and Ms. Casey E. Oswant at the  
593 University of Arizona for proof reading the manuscript. The ~~three~~ anonymous reviewers are  
594 acknowledged for constructive comments and suggestions which helped to improve the  
595 manuscript.

596

597 **References**

- 598 ~~Ackerman, A. S., Kirkpatrick, M. P., Stevens, D. E., and Toon, O. B.: The impact of humidity~~  
599 ~~above stratiform clouds on indirect aerosol climate forcing, *Nature*, 432, 1014–1017, 2004.~~
- 600 Ahlgrim, M., and Forbes, R.: Improving the Representation of Low Clouds and Drizzle in  
601 the ECMWF Model Based on ARM Observations from the Azores, *J. Clim.*, doi:  
602 10.1175/MWR-D-13-00153.1, 2014.
- 603 ~~Albrecht, B. A.: Aerosols, cloud microphysics, and fractional cloudiness, *Science*, 245, 1227–~~  
604 ~~1231, 1989.~~
- 605 Albrecht, B., Fairall, C., Thomson, D., White, A., Snider, J., and Schubert, W.: Surface-based  
606 remote-sensing of the observed and the adiabatic liquid water-content of stratocumulus  
607 clouds, *Geophys. Res. Lett.*, 17, 89–92, doi:10.1029/G1017i001p00089, 1990.
- 608 Austin, P., Wang, Y., Kujala, V., and Pincus, R.: Precipitation in Stratocumulus Clouds:  
609 Observational and Modeling Results, *J. Atmos. Sci.*, 52, 2329–2352, doi:10.1175/1520-  
610 0469(1995)052<2329:PISCOA>2.0.CO;2, 1995.
- 611 Bai, H., Gong, C., Wang, M., Zhang, Z., and L'Ecuyer, T.: Estimating precipitation  
612 susceptibility in warm marine clouds using multi-sensor aerosol and cloud products from  
613 A-Train satellites, *Atmos. Chem. Phys.*, 18, 1763-1783, [https://doi.org/10.5194/acp-18-](https://doi.org/10.5194/acp-18-1763-2018)  
614 [1763-2018](https://doi.org/10.5194/acp-18-1763-2018), 2018.
- 615 Barker H. W., Wiellicki B.A., Parker L.: A parameterization for computing grid-averaged solar  
616 fluxes for inhomogeneous marine boundary layer clouds. Part II: Validation using satellite  
617 data. *J. Atmos. Sci.* 53: 2304–2316, 1996.
- 618 Beheng, K. D.: A parameterization of warm cloud microphysical conversion processes, *Atmos.*  
619 *Res.*, 33, 193-206, 1994.

620 Bony, S., and Dufresne, J.-L.: Marine boundary layer clouds at the heart of tropical cloud  
621 feedback uncertainties in climate models, *Geophys. Res. Lett.*, 32, L20806,  
622 doi:10.1029/2005GL023851, 2005.

623 Boutle, I. A., Abel, S. J., Hill, P. G., and Morcrette, C. J.: Spatial variability of liquid cloud and  
624 rain: Observations and microphysical effects. *Quart. J. Roy. Meteor. Soc.*, 140, 583–594,  
625 doi:10.1002/qj.2140, 2014.

626 Chen, T., Rossow, W. B., and Zhang, Y.: Radiative Effects of Cloud-Type Variations, *J. Clim.*,  
627 13, 264–286, 2000.

628 Cheng, A., and Xu. K.-M.: A PDF-based microphysics parameterization for simulation of  
629 drizzling boundary layer clouds, *J. Atmos. Sci.*, 66, 2317–2334,  
630 doi:10.1175/2009JAS2944.1, 2009.

631 Comstock, K. K., Yuter, S. E., Wood, R., and Bretherton, C. S.: The Three-Dimensional  
632 Structure and Kinematics of Drizzling Stratocumulus, *Mon. Weather Rev.*, 135, 3767–  
633 3784, doi:10.1175/2007MWR1944.1, 2007.

634 Dong X., Ackerman, T. P., and Clothiaux, E. E.: Parameterizations of Microphysical and  
635 Radiative Properties of Boundary Layer Stratus from Ground-based measurements, *J.*  
636 *Geophys. Res.*, 102, 31,681-31,393, 1998.

637 Dong, X., Minnis, P., Ackerman, T. P., Clothiaux, E. E., Mace, G. G., Long, C. N., and  
638 Liljegren, J. C.: A 25-month database of stratus cloud properties generated from ground-  
639 based measurements at the ARM SGP site, *J. Geophys. Res.*, 105, 4529-4538, 2000.

640 Dong, X., Xi, B., Kennedy, A., Minnis, P. and Wood, R.: A 19-month Marine Aerosol-  
641 Cloud\_Radiation Properties derived from DOE ARM AMF deployment at the Azores:  
642 Part I: Cloud Fraction and Single-layered MBL cloud Properties, *J. Clim.*, 27,  
643 doi:10.1175/JCLI-D-13-00553.1, 2014a.



644 Dong, X., Xi, B., and Wu, P.: Investigation of Diurnal Variation of MBL Cloud Microphysical  
645 Properties at the Azores, *J. Clim.*, 27, 8827-8835, 2014b.

646 Fielding, M. D., Chiu, J. C., Hogan, R. J., Feingold, G., Eloranta, E., O'Connor, E. J. and  
647 Cadeddu, M. P.: Joint retrievals of cloud and drizzle in marine boundary layer clouds using  
648 ground-based radar, lidar and zenith radiances. *Atmospheric Measurement Techniques*, 8,  
649 pp. 2663-2683. ISSN 1867-8548 doi: 10.5194/amt-8-2663-2015, 2015.

650 Frisch, A., Fairall, C., and Snider, J.: Measurement of stratus cloud and drizzle parameters in  
651 ASTEX with a Ka-band Doppler radar and a microwave radiometer, *J. Atmos. Sci.*, 52,  
652 2788–2799, 1995.

653 [Geoffroy, O., Brenguier, J.-L., and Burnet, F.: Parametric representation of the cloud droplet  
654 spectra for LES warm bulk microphysical schemes. \*Atmos. Chem. Phys.\*, 10, 4835-4848,  
655 <https://doi.org/10.5194/acp-10-4835-2010>, 2010.](#)

656 Hahn, C. and Warren, S.: A gridded climatology of clouds over land (1971–96) and ocean  
657 (1954–97) from surface observations worldwide, Numeric Data Package NDP-026E  
658 ORNL/CDIAC-153, CDIAC, Department of Energy, Oak Ridge, Tennessee, 2007.

659 Hartmann, D. L., Ockert-Bell, M. E., and Michelsen, M. L.: The Effect of Cloud Type on  
660 Earth's Energy Balance: Global Analysis, *J. Climate*, 5, 1281–1304,  
661 [https://doi.org/10.1175/15200442\(1992\)005<1281:TEOCTO>2.0.CO;2](https://doi.org/10.1175/15200442(1992)005<1281:TEOCTO>2.0.CO;2), 1992.

662 Hartmann, D. L. and Short, D. A.: On the use of earth radiation budget statistics for studies of  
663 clouds and climate, *J. Atmos. Sci.*, 37, 1233–1250, doi:10.1175/1520-  
664 0469(1980)037<1233:OTUOER>2.0.CO;2, 1980.

665 Hill, P. G., Morcrette, C. J., and Boutle, I. A.: A regime-dependent parametrization of subgrid-  
666 scale cloud water content variability, *Q. J. R. Meteorol. Soc.*, 141, 1975–1986, 2015.

667 Houghton, J. T., Ding, Y., Griggs, D.J., Noguer, M., van der Linden, P.J., Dai, X., Maskell, K.,  
668 and Johnson, C.A.: *Climate Change: The Scientific Basis*, Cambridge University Press,  
669 881 pp, 2001.

670 Jess, S.: Impact of subgrid variability on large-scale precipitation formation in the climate  
671 model ECHAM5, PhD thesis, Dep. of Environ. Syst. Sci., ETH Zurich, Zurich,  
672 Switzerland, 2010.

673 Jiang, J., Su, H., Zhai, C., Perun, V. S., Del Genio, A., Nazarenko, L. S., Donner, L. J.,  
674 Horowitz, Seman, L., Cole, C. J., Gettelman, A., Ringer, M. A., Rotstayn, L., Jeffrey, S.,  
675 Wu, T., Brient, F., Dufresne, J-L., Kawai, H., Koshiro, T., Watanabe, M., LÉcuyer, T. S.,  
676 Volodin, E. M., Iversen, Drange, T., H., Mesquita, M. D. S., Read, W. G., Waters, J. W.,  
677 Tian, B., Teixeira, J., and Stephens, G. L.: Evaluation of cloud and water vapor simulations  
678 in CMIP5 climate models using NASA ‘‘A-train’’ satellite observations, *J. Geophys. Res.*,  
679 117, D14105, doi:10.1029/2011JD017237, 2012.

680 Kessler, E.: On the distribution and continuity of water substance in atmospheric circulations,  
681 *Met. Monograph* 10, No. 32, American Meteorological Society, Boston, USA, 84 pp.,  
682 1969.

683 Khairoutdinov, M. and Kogan, Y.: A New Cloud Physics Parameterization in a Large-Eddy  
684 Simulation Model of Marine Stratocumulus, *Mon. Wea. Rev.*, 128, 229-243, 2000.

685 Kooperman, G. J., Pritchard, M. S., Ghan, S. J., Wang, M., Somerville, R. C., and Russell, L.  
686 M.: Constraining the influence of natural variability to improve estimates of global aerosol  
687 indirect effects in a nudged version of the Community Atmosphere Model 5, *J. Geophys.*  
688 *Res.*, 117, D23204, <https://doi.org/10.1029/2012JD018588>, 2012.

689 Kubar, T. L., Hartmann, D. L., and Wood, R.: Understanding the importance of microphysics  
690 and macrophysics in marine low clouds, Part I: satellite observations. *J. Atmos. Sci.*, 66,  
691 2953-2972, doi: 10.1175/2009JAS3071.1, 2009.

692 Larson, V. E., Nielsen, B. J., Fan, J., and Ovchinnikov, M.: Parameterizing correlations  
693 between hydrometeor species in mixed-phase Arctic clouds, *J. Geophys. Res.*, 116,  
694 D00T02, doi:10.1029/2010JD015570, 2011.

695 Larson, V. E., and Griffin, B. M.: Analytic upscaling of a local microphysics scheme. Part I:  
696 Derivation. *Quart. J. Roy. Meteor. Soc.*, 139, 46–57, 2013.

697 Lebsock, M. D., Morrison, H., and Gettelman, A.: Microphysical implications of cloud-  
698 precipitation covariance derived from satellite remote sensing, *J. Geophys. Res.-Atmos.*,  
699 118, 6521–6533, <https://doi.org/10.1002/jgrd.50347>, 2013.

700 Lee, H., and Baik, J.-J.: A physically based autoconversion parameterization. *Journal of the*  
701 *Atmospheric Sciences*, 74, 1599–1616, 2017.

702 Leon, D. C., Wang, Z., and Liu, D.: Climatology of drizzle in marine boundary layer clouds  
703 based on 1 year of data from CloudSat and Cloud-Aerosol Lidar and Infrared Pathfinder  
704 Satellite Observations (CALIPSO), *J. Geophys. Res.*, 113, D00A14,  
705 doi:10.1029/2008JD009835, 2008.

706 Liljegren, J. C., Clothiaux, E. E., Mace, G. G., Kato, S., and Dong, X.: A new retrieval for  
707 cloud liquid water path using a ground-based microwave radiometer and measurements of  
708 cloud temperature, *J. Geophys. Res.*, 106, 14,485-14,500, 2001.

709 Liu, Y. and Daum, P. H.: Parameterization of the autoconversion process, Part I: Analytical  
710 formulation of the Kessler-type parameterizations, *J. Atmos. Sci.*, 61, 1539–1548, 2004.

711 Liu, Y., Daum, P. H., and McGraw, R.: Parameterization of the autoconversion process. Part  
712 II: Generalization of Sundqvist-type parameterizations, *J. Atmos. Sci.*, 63, 1103–1109,  
713 2006a.

714 Liu, Y., Daum, P. H., McGraw, R., Miller, M.: Generalized threshold function accounting for  
715 effect of relative dispersion on threshold behavior of autoconversion process. *Geophys.*  
716 *Res. Lett.*, 33, L11804, 2006b.

717 ~~Lohmann, U. and Feichter, J.: Global indirect aerosol effects: a review, *Atmos. Chem. Phys.*,~~  
718 ~~5, 715–737, doi:10.5194/acp-5-715-2005, 2005.~~

719 Michibata, T., and Takemura, T.: Evaluation of autoconversion schemes in a single model  
720 framework with satellite observations, *J. Geophys. Res. Atmos.*, 120, 9570–9590,  
721 doi:10.1002/2015JD023818, 2015.

722 Miles, N. L., Verlinde, J., and Clothiaux, E. E.: Cloud-droplet size distributions in low-level  
723 stratiform clouds. *J. Atmos. Sci.*, 57, 295–311, doi:10.1175/1520-0469(2000)057,  
724 0295:CDSDIL.2.0.CO;2, 2000.

725 Morrison, H. and Gettelman, A.: A new two-moment bulk stratiform cloud microphysics  
726 scheme in the Community Atmosphere Model, version 3 (CAM3). Part I: Description and  
727 numerical tests, *J. Climate*, 21, 3642–3659, 2008.

728 Nam, C., and Quaas, J.: Evaluation of clouds and precipitation in the ECHAM5 general  
729 circulation model using CALIPSO and CloudSat satellite data, *J. Clim.*, 25, 4975–4992,  
730 doi:10.1175/JCLI-D-11-00347.1, 2012.

731 O’Connor, E. J., Hogan, R. J., and Illingworth, A. J.: Retrieving stratocumulus drizzle  
732 parameters using Doppler radar and lidar, *J. of Applied Meteorol.*, 44, 14-27, 2005.

733 Pincus, R., McFarlane, S. A., and Klein, S. A.: Albedo bias and the horizontal variability of  
734 clouds in subtropical marine boundary layers: Observations from ships and satellites, *J.*  
735 *Geophys. Res.*, 104, 6183–6191, doi:10.1029/1998JD200125, 1999.

736 Pincus, R., and Klein, S. A.: Unresolved spatial variability and microphysical process rates in  
737 large-scale models. *J. Geophys. Res.*, 105D, 27 059–27 065, 2000.

738 Quaas, J., Ming, Y., Menon, S., Takemura, T., Wang, M., Penner, J. E., Gettelman, A.,  
739 Lohmann, U., Bellouin, N., Boucher, O., Sayer, A. M., Thomas, G. E., McComiskey, A.,  
740 Feingold, G., Hoose, C., Kristjánsson, J. E., Liu, X., Balkanski, Y., Donner, L. J., Ginoux,  
741 P. A., Stier, P., Grandey, B., Feichter, J., Sednev, Bauer, S. E., Koch, D., Grainger, R. G.,  
742 Kirkevåg, A., Iversen, T., Seland, Ø., Easter, R., Ghan, S. J., Rasch, P. J., Morrison, H.,  
743 Lamarque, J.-F., Iacono, M. J., Kinne, S., and Schulz, M.: Aerosol indirect effects –

744 general circulation model intercomparison and evaluation with satellite data, *Atmos.*  
745 *Chem. Phys.*, 9, 8697–8717, <https://doi.org/10.5194/acp-9-8697-2009>, 2009.

746 Randall, D. A., Coakley, J. A., Fairall, C. W., Knopfli, R. A., and Lenschow, D. H.: Outlook  
747 for research on marine subtropical stratocumulus clouds. *Bull. Amer. Meteor. Soc.*, 65,  
748 1290–1301, 1984.

749 Rémillard, J., Kollias, P., Luke, E., and Wood, R.: Marine Boundary Layer Cloud Observations  
750 in the Azores, *J. Climate*, 25, 7381–7398, doi: [http://dx.doi.org/10.1175/JCLI-D-11-](http://dx.doi.org/10.1175/JCLI-D-11-00610.1)  
751 [00610.1](http://dx.doi.org/10.1175/JCLI-D-11-00610.1), 2012.

752 Rémillard, J., Kollias, P., and Szyrmer, W.: Radar-radiometer re-  
753 trievals of cloud number concentration and dispersion parameter in nondrizzling marine stratocumulus, *Atmos.*  
754 *Meas. Tech.*, 6, 1817–1828, doi:10.5194/amt-6-1817-2013, 2013.

755 Slingo, A.: Sensitivity of the Earth’s radiation budget to changes in low clouds, *Nature*, 343,  
756 49–51, <https://doi.org/10.1038/343049a0>, 1990.

757 Song, H., Zhang, Z., Ma, P.-L., Ghan, S. J., and Wang, M.: An Evaluation of Marine Boundary  
758 Layer Cloud Property Simulations in the Community Atmosphere Model Using Satellite  
759 Observations: Conventional Subgrid Parameterization versus CLUBB, *J. Clim.*,  
760 doi:10.1175/JCLI-D-17-0277.1, 2018.

761 Stanfield, R., Dong, X., Xi, B., Gel Genio, A., Minnis, P., and Jiang, J.: Assessment of NASA  
762 GISS CMIP5 and post CMIP5 Simulated Clouds and TOA Radiation Budgets Using  
763 Satellite Observations: Part I: Cloud Fraction and Properties, *J. Clim.*, doi:10.1175/JCLI-  
764 [D-13-00588.1](https://doi.org/10.1175/JCLI-D-13-00588.1), 2014.

765 Tripoli, G. J. and Cotton, W. R.: A numerical investigation of several factors contributing to  
766 the observed variable intensity of deep convection over South Florida., *J. Appl. Meteorol.*,  
767 19, 1037–1063, 1980.

768 Troyan, D.: Merged Sounding Value-Added Product, Tech. Rep., DOE/SC-ARM/TR-087,  
769 2012.

770 Walters, D., Baran, A., Boutle, I., Brooks, M., Earnshaw, P., Edwards, J., Furtado, K., Hill, P.,  
771 Lock, A., Manners, J., Morcrette, C., Mulcahy, J., Sanchez, C., Smith, C., Stratton, R.,  
772 Tennant, W., Tomassini, L., van Weverberg, K., Vosper, S., Willett, M., Browse, J.,  
773 Bushell, A., Dalvi, M., Essery, R., Gedney, N., Hardiman, S., Johnson, B., Johnson, C.,  
774 Jones, A., Mann, G., Milton, S., Rumbold, H., Sellar, A., Ujiie, M., Whittall, M., Williams,  
775 K. and Zerroukat, M. The Met Office Unified Model Global Atmosphere 7.0/7.1 and  
776 JULES Global Land 7.0 configurations. *Geosci. Model Dev.*, doi:10.5194/gmd-2017-291,  
777 2017.

778 Wang, M., Ghan, S., Liu, X., L'Ecuyer, T. S., Zhang, K., Morrison, H., Ovchinnikov, M.,  
779 Easter, R., Marchand, R., Chand, D., Qian, Y., and Penner, J. E.: Constraining cloud  
780 lifetime effects of aerosols using A-Train satellite observations, *Geophys. Res. Lett.*, 39,  
781 L15709, <https://doi.org/10.1029/2012GL052204>, 2012.

782 Warren, S. G., Hahn, C. J., London, J., Chervin, R. M., and Jenne, R.: Global distribution of  
783 total cloud cover and cloud type amount over land, Tech. Rep. Tech. Note TN-317 STR,  
784 NCAR, 1986.

785 Warren, S. G., Hahn, C. J., London, J., Chervin, R. M., and Jenne, R.: Global distribution of  
786 total cloud cover and cloud type amount over land, Tech. Rep. Tech. Note TN-317 STR,  
787 NCAR, 1988.

788 Weber, T., and Quaas, J.: Incorporating the subgrid-scale variability of clouds in the  
789 autoconversion parameterization using a PDF-scheme, *J. Adv. Model. Earth Syst.*, 4,  
790 M11003, doi:10.1029/2012MS000156, 2012.

791 Wielicki, B. A., Cess, R. D., King, M. D., Randall, D. A., and Harrison, E. F.: Mission to planet  
792 Earth: Role of clouds and radiation in climate, *Bull. Amer. Meteor. Soc.*, 76, 2125–2153,  
793 doi:10.1175/1520-0477(1995)076<2125:MTPERO.2.0.CO;2, 1995.

794 [Witte, M. K., Yuan, T., Chuang, P. Y., Platnick, S., Meyer, K. G., Wind, G., and Jonsson, H.](#)  
795 [H.: MODIS retrievals of cloud effective radius in marine stratocumulus exhibit no](#)

796 [significant bias. \*Geophysical Research Letters\*, 45, 10,656–10,664.](#)  
797 <https://doi.org/10.1029/2018GL079325>, 2018.

798 Wood, R., Field, P. R., and Cotton, W. R.: Autoconversion rate bias in stratiform boundary  
799 layer cloud parameterization. *Atmos. Res.*, 65, 109–128, 2002.

800 Wood, R.: Drizzle in stratiform boundary layer clouds. Part I: Vertical and horizontal structure,  
801 *J. Atmos. Sci.*, 62, 3011–3033, 2005a.

802 Wood, R.: Drizzle in stratiform boundary layer clouds. Part II: Microphysical aspects, *J.*  
803 *Atmos. Sci.*, 62, 3034–3050, 2005b.

804 Wood, R. and Hartmann, D.: Spatial variability of liquid water path in marine low cloud: The  
805 importance of mesoscale cellular convection, *J. Climate*, 19, 1748–1764, 2006.

806 Wood, R.: Cancellation of aerosol indirect effects in marine stratocumulus through cloud  
807 thinning. *J. Atmos. Sci.*, 64, 2657–2669, 2007.

808 Wood, R.: Stratocumulus Clouds, *Mon. Wea. Rev.*, 140, 2373–2423. doi:  
809 <http://dx.doi.org/10.1175/MWR-D-11-00121.1>, 2012.

810 Wood, R., Wyant, M., Bretherton, C. S., Rémillard, J., Kollias, P., Fletcher, J., Stemmler, J.,  
811 deSzoek, S., Yuter, S., Miller, M., Mechem, D., Tselioudis, G., Chiu, C., Mann, J.,  
812 O'Connor, E., Hogan, R., Dong, X., Miller, M., Ghate, V., Jefferson, A., Min, Q., Minnis,  
813 P., Palinkonda, R., Albrecht, B., Luke, E., Hannay, C., Lin, Y.: Clouds, Aerosol, and  
814 Precipitation in the Marine Boundary Layer: An ARM Mobile Facility Deployment, *Bull.*  
815 *Amer. Meteorol. Soc.*, doi: <http://dx.doi.org/10.1175/BAMS-D-13-00180.1>, 2015.

816 Wu, P., Dong, X. and Xi, B.: Marine boundary layer drizzle properties and their impact on  
817 cloud property retrieval, *Atmos. Meas. Tech.*, 8, 3555–3562. doi: 10.5194/amt-8-3555-  
818 2015, 2015.

819 Wu, P., Dong, X., Xi, B., Liu, Y., Thieman, M., and Minnis, P.: Effects of environment forcing  
820 on marine boundary layer cloud-drizzle processes, *J. Geophys. Res. Atmos.*, 122, 4463–  
821 4478, doi:10.1002/2016JD026326, 2017.

822 Xie, X., and Zhang, M.: Scale-aware parameterization of liquid cloud inhomogeneity and its  
823 impact on simulated climate in CESM, *J. Geophys. Res. Atmos.*, 120, 8359–8371,  
824 doi:10.1002/2015JD023565, 2015.

825 Yoo, H., and Li, Z.: Evaluation of cloud properties in the NOAA/NCEP Global Forecast  
826 System using multiple satellite products. *Climate Dyn.*, 39, 2769–2787,  
827 doi:10.1007/s00382-012-1430-0, 2012.

828 Yoo, H., and Li, Z., Hou, Y.-T., Lord, S., Weng, F., and Barker, H. W.: Diagnosis and testing  
829 of low-level cloud parameterizations for the NCEP/GFS using satellite and ground-based  
830 measurements. *Climate Dyn.*, 41, 1595–1613, doi:10.1007/s00382-013-1884-8, 2013.

831 Zhang, J., Lohmann, U., and Lin, B.: A new statistically based autoconversion rate  
832 parameterization for use in large-scale models. *J. Geophys. Res.*, 107, 4750,  
833 doi:10.1029/2001JD001484, 2002.

834 Zhang, Z., Song, H., Ma, P.-L., Larson, V., Wang, M., Dong, X., and Wang, J.: Subgrid  
835 variations of cloud water and droplet number concentration over tropical oceans: satellite  
836 observations and implications for warm rain simulation in climate models. Submitted to  
837 *Atmos. Chem. Phys.*, 2018.

838



839 **Table 1. The parameters of autoconversion and accretion formulations for four**  
840 **parameterizations.**  
841

|                                   | $A$   | $a1$ | $a2$  | $B$ | $b$  |
|-----------------------------------|---|------|-------|-----|------|
| Khairoutdinov and<br>Kogan (2000) | 1350  | 2.47 | -1.79 | 67  | 1.15 |
| Liu and Daum (2004)               | $1.3 \times 10\beta_6^6$ ,<br>where $\beta_6^6 = [(r_v + 3)/r_v]^2$ ,<br>$r_v$ is mean volume radius.<br>modification was made by<br>Wood (2005b) | 3    | -1    | N/A | N/A  |
| Tripoli and Cotton<br>(1980)      | 3268  | 7/3  | -1/3  | 1   | 1    |
| Beheng (1994)                     | $3 \times 10^{34}$ for $N_c < 200 \text{ cm}^{-3}$<br>$9.9$ for $N_c > 200 \text{ cm}^{-3}$   | 4.7  | -3.3  | 1   | 1    |

842

843 **Table 2. Autoconversion (left) and accretion (right) enhancement factors in different**  
 844 **boundary layer conditions (LTS > 18 K for stable, LTS < 13.5 K for unstable and LTS**  
 845 **within 13.5 and 18 K for mid-stable) and in different LWP regimes (LWP ≤ 75 g m<sup>-2</sup> for**  
 846 **non-precipitating and LWP > 75 g m<sup>-2</sup> for precipitating).**

847

| <u>LTS (K)</u>                       | LWP ≤ 75 g m <sup>-2</sup> | LWP > 75 g m <sup>-2</sup> |
|--------------------------------------|----------------------------|----------------------------|
| > 18 <u>K</u>                        | 2.32/1.42                  | 2.75/1.52                  |
| <u>(13.5, ≤ LTS ≤</u><br><u>18K)</u> | 2.61/1.47                  | 3.07/1.68                  |
| <u>LTS &lt; 13.5 K</u>               | 4.62/1.72                  | 6.94/1.86                  |

Formatted Table

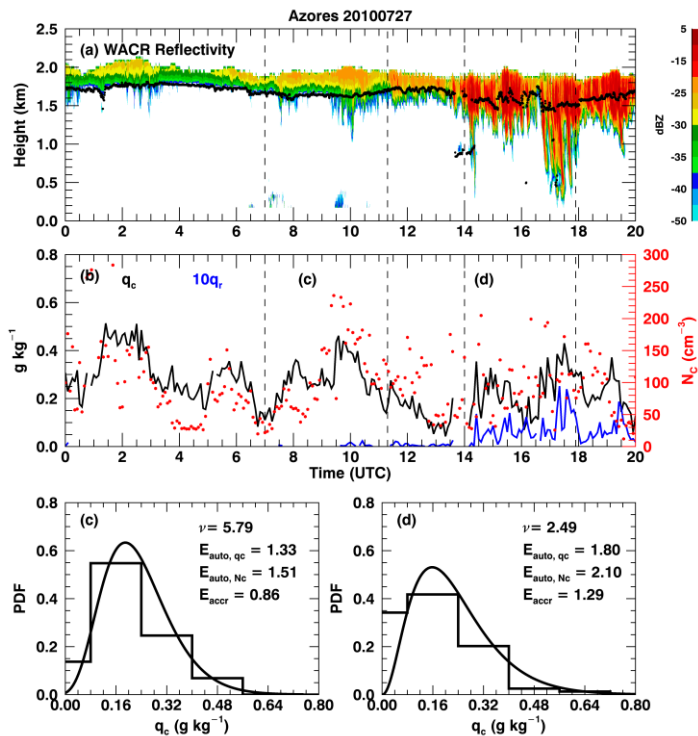
848

849 **Table 3. Autoconversion and accretion enhancement factors ( $E_{auto}$  and  $E_{accr}$ ) for the**  
 850 **parameterizations in Table 1 except the Khairoutdinov and Kogan (2000) scheme. The**  
 851 **values are averaged for 60-km and 180-km equivalent size model grids.**  
 852

Formatted: Font: Bold

|                              | $E_{auto}$ |        | $E_{accr}$ |        |
|------------------------------|------------|--------|------------|--------|
|                              | 60-km      | 180-km | 60-km      | 180-km |
| Liu and Daum (2004)          | 3.82       | 4.23   | N/A        | N/A    |
| Tripoli and Cotton<br>(1980) | 2.46       | 2.69   | 1.47       | 1.56   |
| Beheng (1994)                | 6.94       | 5.88   | 1.47       | 1.56   |

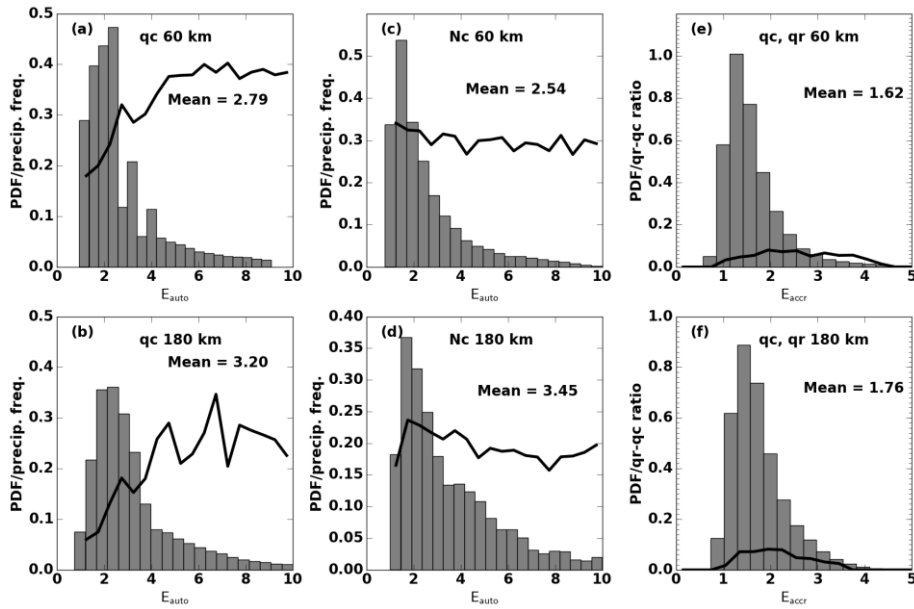
853



854

855 Figure 1. Observations and retrievals over Azores on 27 July 2010. (a) W-band ARM  
 856 cloud radar (WACR) reflectivity (contour) superimposed with cloud-base height (black  
 857 dots). (b) Black line represents averaged cloud water mixing ratio ( $q_c$ ) within the top five  
 858 range gates, blue line represents averaged rain ( $\times 10$ ) water mixing ratio within five range  
 859 gates around maximum reflectivity, red dots are the retrieved cloud droplet number  
 860 concentration ( $N_c$ ). Dashed lines represent two periods that have 60 km **equivalent model**  
 861 **grid sizes** with similar  $\overline{q_c}$  mean  $q_c$  but different distributions as shown by step lines in (c)  
 862 and (d). Curved lines in (c) and (d) are fitted gamma distributions with the corresponding  
 863 shape parameter ( $\nu$ ) shown on the upper right.  $N_c$  distributions are not shown. The  
 864 calculated autoconversion ( $E_{\text{auto}, q_c}$  from  $q_c$  and  $E_{\text{auto}, N_c}$  from  $N_c$ ) and accretion ( $E_{\text{accr}}$ )  
 865 enhancement factors are also shown.

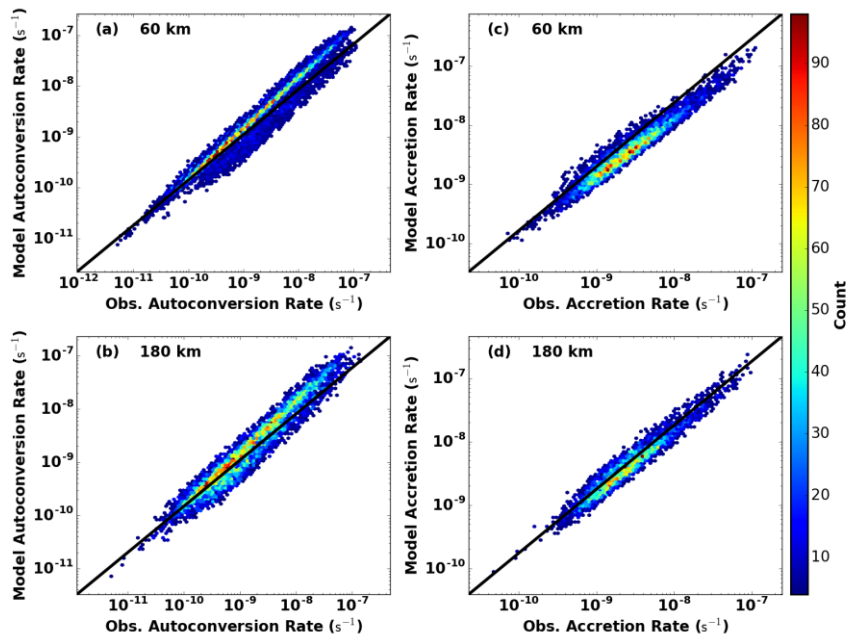
866  
867



868

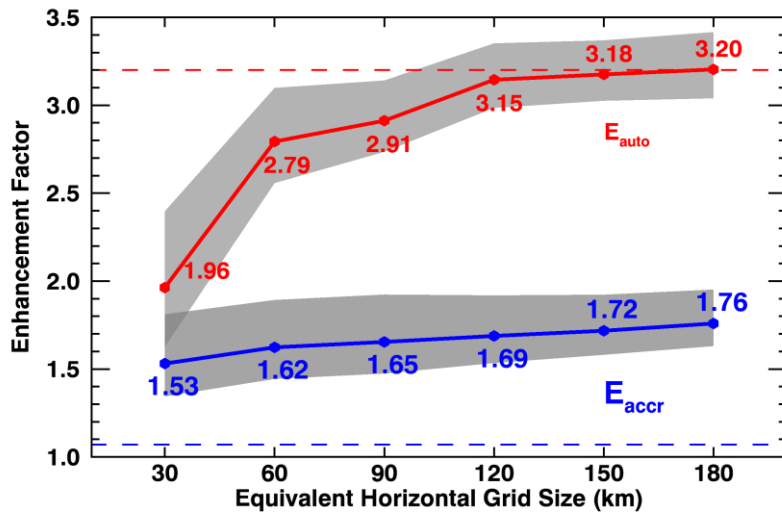
869 **Figure 2. Probability density functions (PDFs) of autoconversion (a - d) and accretion (e**  
870 **- f) enhancement factors calculated from  $q_c$  (a-b),  $N_c$  (c-d), and the covariance of  $q_c$  and**  
871  **$q_r$  (e-f). The two rows show the results from 60-km equivalent model**  
872 **gridsizes, respectively, with their average values. Black lines represent precipitation**  
873 **frequency in each bin in (a)-(d) and the ratio of layer-mean  $q_r$  to  $q_c$  in (e)-(f).**

874



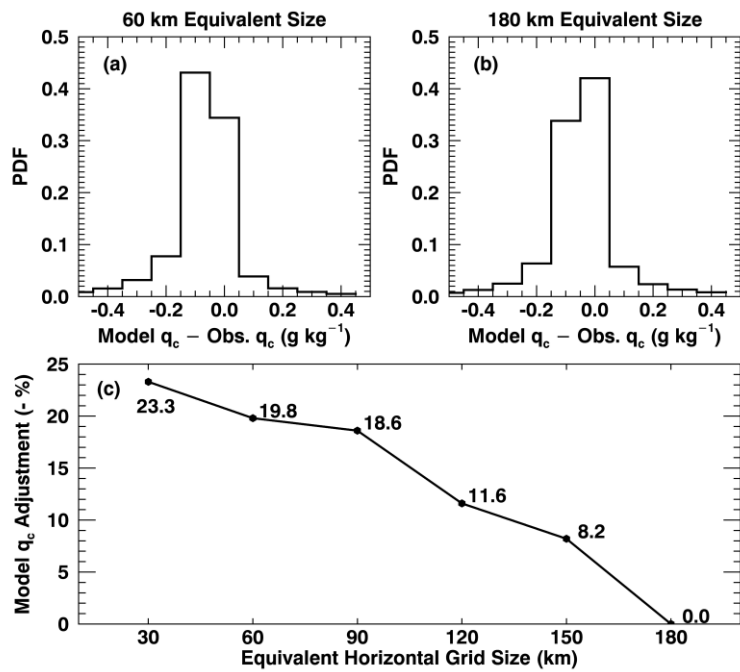
875

876 Figure 3. Comparison of autoconversion (a-b) and accretion (c-d) rates derived from  
 877 observations (x-axis) and from model (y-axis). Results are for 60-km (a and c) and 180-  
 878 km model equivalent grid sizes. Colored dots represent joint number densities.



880 Figure 4. Autoconversion (red line) and accretion (blue line) enhancement factors as a  
 881 function of equivalent model grid sizes. The shaded areas are calculated by varying  $q_c$   
 882 and  $q_r$  within their retrieval uncertainties. The two dashed lines show the constant values  
 883 of autoconversion (3.2) and accretion (1.07) enhancement factors prescribed in MG08.

884

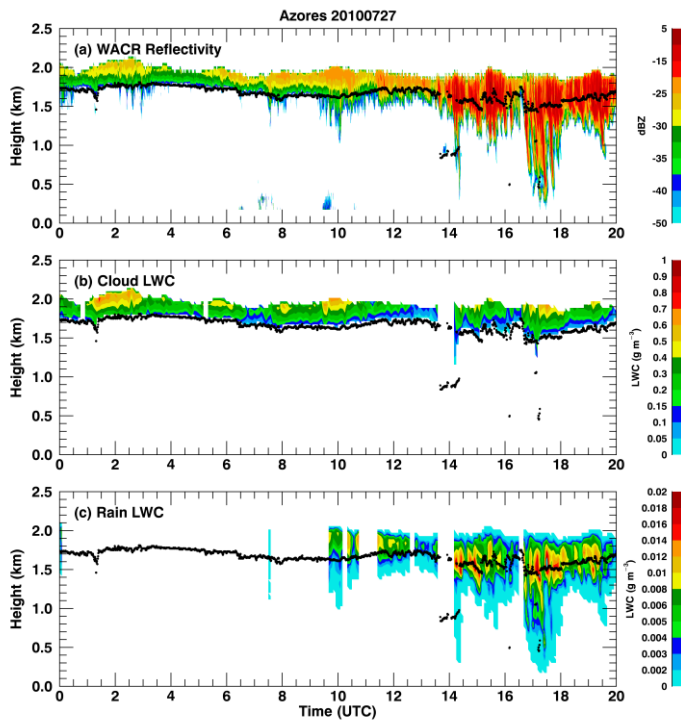


885

886 Figure 5.  $q_c$  needed for models to adjust to reach the same autoconversion rate as  
 887 observations for (a) 60-km and (b) 180-km model equivalent grid sizes. Positive biases  
 888 represent increased  $q_c$  are required in models and negative biases mean decreased  $q_c$ . The  
 889 average percentages of adjustments for different equivalent model grid sizes are shown  
 890 in panel (c) and note that the percentages in the vertical axis are negative.

891





892

893 **Figure A1. Joint retrieval of cloud and rain liquid water content (CLWC and RLWC) for**  
 894 **the same case as in Figure 1. (a) WACR reflectivity, (b) CLWC, and (c) RLWC. The black**  
 895 **dots represent cloud base height. Blank gaps are due to the data from one or more**  
 896 **observations are not available or reliable. For example, the gap before 14 UTC is due to**  
 897 **multiple cloud layers are detected whereas we only focus on single layer cloud.**